NATIONAL ADVISORY COMMITTEE
FOR AERONAUTICS

TECHNICAL NOTE 2474

EMPIRICAL RELATION BETWEEN INDUCED VELOCITY, THRUST,

AND RATE OF DESCENT OF A HELICOPTER ROTOR AS

DETERMINED BY WIND-TUNNEL TESTS

ON FOUR MODEL ROTORS

By Walter Castles, Jr. and Robin B. Gray

Georgia Institute of Technology

NACA

Washington

October 1951

1

NATIONAL ADVISORY COMMITTEE FOR AERONAUTICS

TECHNICAL NOTE 2474

EMPIRICAL RELATION BETWEEN INDUCED VELOCITY, THRUST,

AND RATE OF DESCENT OF A HELICOPTER ROTOR AS

DETERMINED BY WIND-TUNNEL TESTS

ON FOUR MODEL ROTORS

By Walter Castles, Jr. and Robin B. Gray

SUMMARY

The empirical relation between the induced velocity, thrust, and rate of vertical descent of a helicopter rotor was calculated from wind-tunnel force tests on four model rotors by the application of blade-element theory to the measured values of the thrust, torque, blade angle, and equivalent free-stream rate of descent.

The model tests covered the useful range of C_T/σ_e (where C_T is the thrust coefficient and σ_e, the effective solidity) and the range of vertical descent from hovering to descent velocities slightly greater than those for autorotation.

The three bladed models, each of which had an effective solidity of 0.05 and NACA 0015 blade airfoil sections, were as follows:

(1) Constant-chord, untwisted blades of 3-foot radius

(2) Untwisted blades of 3-foot radius having a 3/1 taper

(3) Constant-chord blades of 3-foot radius having a linear twist of 12° (washout) from axis of rotation to tip

(4) Constant-chord, untwisted blades of 2-foot radius.

Because of the incorporation of a correction for blade dynamic twist and the use of a method of measuring the approximate equivalent free-stream velocity, it is believed that the data obtained from this program are more applicable to free-flight calculations than the data from previous model tests.

The results of the tests are presented in the form of graphs of the nondimensional induced velocity λ_i against the nondimensional

rate of vertical descent λ_z, rather than in the usual form of Glauert's curve of $1/f$ against $1/F$ (where f is the thrust coefficient based on descent velocity and F, the thrust coefficient based on the resultant velocity at the rotor) as it is believed that the former form more clearly expresses the physical significance of the results.

In order to determine the approximate rotor flow patterns, the longitudinal cross section of the wind-tunnel jet was tufted on vertical wires, and a photograph of the tufts was obtained at each test point. Also, eight smoke filaments were injected along a radial line 9 inches above the rotor plane and photographed along with the jet tufts for a complete run at $C_T = 0.004$ on the small rotor.

The following general observations may be made from these tests:

(1) The mean nondimensional induced velocities calculated from the present test data are considerably less for hovering and the smaller rates of descent and considerably larger for the higher rates of descent than those given by Glauert's curve of $1/f$ against $1/F$. The nondimensional induced velocities obtained in the present tests are in good agreement with the values obtained from full-scale data at the hovering and autorotation ends of the vertical-descent range but are higher than the full-scale values reported by Stewart at the larger rates of power-on descent.

(2) The present tests indicate that the primary effect of a 3/1 blade taper is to reduce slightly the values of the nondimensional induced velocity at hovering and the small rates of descent and to increase the rate of descent for "ideal" autorotation, that rate of descent at which the induced and descent velocities are equal, by approximately 3 percent as compared with a rotor having constant-chord, untwisted blades.

(3) Linear blade twist of 12° also slightly reduced the value of the nondimensional induced velocity at hovering in comparison with the value obtained on the rotor with the constant-chord, untwisted blades. The twist increased the "ideal" rate of descent for autorotation by approximately 10 percent. Also the peak value of the nondimensional induced velocity was increased by approximately 24 percent over that for the rotor with constant-chord, untwisted blades, and the peak occurred at a rate of descent that was about 17 percent higher.

The fluctuations in the forces and moments on the rotor with the twisted blades were very much larger at the higher rates of power-on descent than those for the rotors with tapered or constant-chord, untwisted blades.

(4) Within the range and accuracy of the present tests there were no significant differences in the values of λ_i at given values of λ_z that could be attributed to the variations in the test thrust coefficient, rotor angular velocity, or rotor diameter.

INTRODUCTION

Contemporary vortex or momentum theory does not yield a useful answer for the mean induced velocity of a helicopter rotor in vertical descent because of the limited and indefinite extent of the rotor wake. Thus the relation between the mean induced velocity, thrust, and rate of vertical descent must, at present, be determined experimentally.

Both wind-tunnel and flight tests, the only readily available experimental methods of determining the empirical induced-velocity relation for vertical descent, offer certain difficulties. It is not easy to maintain the desired zero horizontal component of velocity on flight tests or to measure the rate of descent with sufficient accuracy. Also, existing helicopters tend to suffer a loss of control at the larger rates of power-on descent and thus it is hard to obtain steady-state flight data in this range. Wind-tunnel model rotor tests, on the other hand, present certain problems in determining the equivalent free-stream descent velocities corresponding to the test conditions and also in measuring or deducing the operating rotor blade angles.

Recent flight-test data have been in serious disagreement with the only previous wind-tunnel test data, and Glauert's empirical induced-velocity relation, $1/f$ against $1/F$, based on the results of this test. This disagreement has cast certain doubts on the usefulness of wind-tunnel model rotor tests in general.

The present test program was undertaken in an effort to check Glauert's curve of $1/f$ against $1/F$ over the useful range of vertical descent and, if possible, to find the sources of discrepancy between the model and free-flight results. It was also desired to evaluate the principal effects of blade taper and twist on the vertical-descent characteristics and to obtain a sequence of smoke filament and tuft photographs to show the approximate flow patterns.

A reexamination of the test methods and the procedure used to reduce the data for Glauert's curve of $1/f$ against $1/F$ indicated that the probable sources of error in the results were due to the use of a wind tunnel having a closed test section and an energy ratio considerably greater than unity, the determination of the equivalent free-stream descent velocity from a pressure tap in the tunnel wall, and the neglect of the dynamic twist of the blades. The present tests

covering the useful range of C_T/σ_e and vertical descent on the afore-mentioned four rotors were designed to eliminate, insofar as possible, the above errors.

This work was conducted at the Georgia Institute of Technology under the sponsorship and with the financial assistance of the National Advisory Committee for Aeronautics.

SYMBOLS

a   blade-element lift-curve slope

A   rotor-disk area

b   number of blades in rotor

c   blade-element chord

c_{d_o} blade-element profile drag coefficient

c_e equivalent blade chord $\left(\dfrac{\displaystyle\int_0^R cr^2\,dr}{\displaystyle\int_0^R r^2\,dr} \right)$

c_l blade-element lift coefficient

c_o extended blade root chord

C_T thrust coefficient $\left(T/\rho\pi\Omega^2 R^4 \right)$

C_Q torque coefficient $\left(Q/\rho\pi\Omega^2 R^5 \right)$

ΔC_Q increment in torque coefficient over that for zero thrust and zero rate of descent

f thrust coefficient based on descent velocity $\left(T/2\rho\pi V^2 R^2\right)$; usually found in differential form $\left(\dfrac{1}{4\rho\pi V^2 r}\dfrac{dT}{dr}\right)$

F thrust coefficient based on resultant velocity at rotor $\left(\dfrac{T}{2\rho\pi\left(V_i \pm V\right)^2 R^2}\ \text{ or }\ \dfrac{1}{4\rho\pi\left(V_i \pm V\right)^2 r}\dfrac{dT}{dr}\right)$

Q rotor torque

r radius of blade element

R rotor radius

R_e effective radius $\left(R - \dfrac{1}{2}\text{ tip chord}\right)$

t taper factor $\left(\dfrac{c_{tip}}{c_o} - 1\right)$

T rotor thrust

V descent velocity

V_i induced velocity at rotor, measured with respect to fixed coordinates

x nondimensional radius of blade element (r/R)

α_r blade-element angle of attack

$\delta_0,\ \delta_1,\ \delta_2$ coefficients in power series expressing c_{d_o} as function of α_r, where $c_{d_o} = \delta_0 + \delta_1\alpha_r + \delta_2\alpha_r^2$

θ blade-element pitch angle, measured between zero-lift chord line and tip-path plane

θ_o extended blade root pitch angle

θ_1 extended linear twist from axis of rotation to blade tip, positive when tip angle is the larger

θ_0 factor $\left(16\theta_0/a\sigma_0\right)$

θ_1 factor $\left(16\theta_1/a\sigma_0\right)$

λ_i nondimensional induced velocity $\left(\dfrac{V_i}{\Omega R\sqrt{\frac{1}{2}\,C_T}} \quad \text{or} \quad \dfrac{V_i}{\sqrt{T/2\rho A}}\right)$

λ_z nondimensional descent velocity $\left(\dfrac{V}{\Omega R\sqrt{\frac{1}{2}\,C_T}} \quad \text{or} \quad \dfrac{V}{\sqrt{T/2\rho A}}\right)$

ρ mass density of air

σ_e effective solidity $\left(bc_e/\pi R\right)$

σ_0 solidity of extended blade root chord $\left(bc_0/\pi R\right)$

σ_1 solidity factor $\left(\dfrac{b}{\pi R^2}\displaystyle\int_0^R c\,dr\right)$

σ_2 solidity factor $\left(\dfrac{b}{\pi R^3}\displaystyle\int_0^R cr\,dr\right)$

σ_3 solidity factor $\left(\dfrac{b}{\pi R^4}\displaystyle\int_0^R cr^2\,dr\right)$

σ_4 solidity factor $\left(\dfrac{b}{\pi R^5}\displaystyle\int_0^R cr^3\,dr\right)$

σ_5 solidity factor $\left(\dfrac{b}{\pi R^6}\displaystyle\int_0^R cr^4\,dr\right)$

$\varnothing$ inflow angle at blade element, positive below rotor plane

Ω angular velocity of rotor

DESCRIPTION OF APPARATUS

Wind tunnel.- The wind tunnel, in the open jet of which these tests were conducted, is of conventional closed-return type having a 5-to-1 contraction in the collector. The open jet is circular, of 9-foot diameter, and 10 feet long. There is a flat wind-tunnel balance cover just below the bottom boundary of the open jet. The rotors were installed so that the rotor hub was in the transverse and longitudinal center line of the open jet.

For the present tests an 18- by 18-mesh wake-diffusion screen was installed 21 feet downstream of the rotor plane. This screen reduced the tunnel energy ratio to approximately 0.7. In addition, a precision electric tachometer was installed on the wind-tunnel motor and gear driven to read 10 times wind-tunnel propeller shaft speed. This permitted the wind-tunnel propeller speed to be read to ±1/2 revolution per minute.

Rotor test stand.- The rotor test stand is a self-contained unit which mounts in a load member support socket of the normal wind-tunnel balance as shown in figure 1. The power is furnished by a three-phase, 15-horsepower, 1750-revolution-per-minute, wound rotor induction motor. The motor shaft is coupled to the pinion in the gear box contained in the 6-inch-pipe tee by a vertical drive shaft. The pinion drives, at half motor speed, a ring gear to which the differential planetary carrier is attached as shown in figure 2. The rear shaft from the miter gear set in the differential carrier is restrained from rotating by the torque-measuring strain-gage arm. The front shaft from the miter gear set drives the separately supported rotor hub through a ball-bearing slip and universal joint in the center of the rotor. This ball-bearing slip and universal joint can transmit no thrust nor steady moments to the hub other than the driving torque.

The hub is supported and rotates on two ball bearings mounted in a three-arm strain-gage spider, the outer ends of the arms of which are ball-bearing mounted on the test stand. This strain-gage spider, which is entirely within the hub, carries and measures only the thrust force on the rotor and hub. Inside the front of the hub there is a pitch-change motor which screws the outer hub fairing back and forth and through ball-bearing connections changes the pitch of the rotor blades. Extending from the front of this hub fairing is a revolution counter driven by the pitch-change motor shaft. A unit change on this counter, which was read during the tests by means of a stroboscope unit and field glasses, corresponds to a rotor-blade-angle change of 0.041° to 0.043° over the range of blade angles covered in these tests.

The gear box was made of the dry sump type with all units mounted on ball bearings and the gears lubricated by jets of low-viscosity oil furnished by an external oil pump in order to keep the tare torque low and constant.

The thrust and torque strain gages were read by means of SR-4 bridges arranged in temperature compensating circuits. The thrust could be read to approximately ±0.05 pound. The torque on the heavier arm used with the 6-foot-diameter rotors could be read to approximately ±0.004 foot-pound and on the lighter arm used with the 4-foot-diameter rotor, to approximately ±0.002 foot-pound.

The rotor speed was measured by means of a neon flash lamp actuated by a set of breaker points on the motor shaft. This flash lamp illuminated once each rotor revolution a suitably lined disk driven by a small synchronous motor. The rotor speed was continuously manually controlled by means of a three-phase lye barrel rheostat in the motor armature circuit in such a manner that the image of the lined disk on the synchronous motor shaft remained approximately stationary. Assuming that power line frequency was constant, the error in rotor speed was probably not over ±2 revolutions per minute. In order to be certain that the desired image harmonic was the one being controlled, the rotor-drive-motor speed was also read on an electric tachometer.

The tunnel-off tare thrust was not measurable. The tare torque at 1600 revolutions per minute, including windage on the hub and blade sockets, was 0.18 foot-pound and constant after the gears had been run in. In addition, there was a torque loss of approximately 3 percent through the differential miter gear set. The torque loss in the ring and pinion was not reflected in the torque-arm strain-gage reading.

Model rotor blades.- The model rotor blades, each set of which had an effective solidity of 0.05 and NACA 0015 airfoil sections, were of the "rigid" type with no initial coning angle. To keep torsional deflections to a minimum the blades were designed so that the chordwise locations of the centers of gravity, elastic axes, and aerodynamic centers of the blade elements coincided, approximately, and lay on the quarter-chord pitch-change axis.

The large centrifugal loads arising from the full-scale design tip speed and the above-mentioned torsional considerations necessitated building the blades with a solid alloy steel leading edge extending back to approximately the quarter-chord point.

The constant-chord, untwisted blades were constructed with a hollow magnesium trailing-edge section riveted to the steel leading edge as shown in figure 3. The twisted set of blades and the tapered blades were

constructed with solid laminated mahogany trailing-edge sections fastened to the steel leading edge with machine screws. The blades were hand-worked to contour, and the final finish obtained, while not aerodynamically smooth, had no significant imperfections.

The diameter of the hub fairing was $6\frac{1}{4}$ inches. The blades were of true contour from a radius of 6.09 inches out, and the blade tips were finished off square. Rotor static balance was obtained by ring balance weights held in position around the hub blade sockets by set screws.

TEST PROCEDURE

After the installation of the rotor test stand with hub, but without blades, and the tunnel wake-diffusion screen, the speed of the wind-tunnel propeller and tunnel piezometer reading were calibrated against the tunnel jet velocity as measured by a standard pitot tube and micro-manometer. Vertical and horizontal jet-center-line velocity surveys were taken in the plane of rotation. It was found that the jet velocity distribution was satisfactory except for a local region directly ahead of the 5-inch-diameter-rotor test-stand support located 18 inches downstream from the plane of rotation. Within this local region the velocities were $3\frac{1}{2}$ percent below the average.

The procedure for a typical run was as follows: After sufficient warm-up time for the lubricating oil pressure to stabilize, tare thrust and torque readings were obtained on the hub without blades at various rotor speeds and wind-tunnel velocities. The hub was then dismounted, a set of blades installed, and the rotor balanced. The blade angle at the three-quarter-radius point on each blade was then set with a precision inclinometer to within approximately ±2 minutes of equal angles of about 6° by adjusting the clamps on the blade-pitch-change arms. The hub was then reinstalled and the previous calibration of the thrust strain system was checked by wire, pulley, and weights.

The rotor was then brought up to test speed (1200 or 1600 rpm) and, after another warm-up period, a reading was taken of the reference blade angle (counter reading) and torque for zero thrust. The accuracy with which the zero-thrust blade angle could be determined was not too satis-factory, as explained below.

The blade angle was then set by trial and error at the value giving the desired thrust coefficient as indicated by the thrust strain-gage setup, and a reading was taken of the torque and blade angle. In

addition, a photograph was taken of the tufts in the tunnel jet, and a reading was taken of the tunnel velocity indicated by the tunnel piezometer.

The tunnel fan was then started and the above procedure and readings were repeated for each successive increment in tunnel velocity that could be obtained from the taps on the wind-tunnel-motor-armature rheostat. In addition, a reading of the wind-tunnel propeller speed was made for each of these points. The run was terminated at that velocity increment at which the measured torque reached a zero or negative value or, on the small rotor, at a rate of descent known to be in the windmill brake state.

After a descent run at each desired value of C_T was obtained on a given rotor, the tunnel was completely blocked by placing a layer of paper over the wake-diffusion screen. A hovering test run, reading thrust and torque against blade angle, was then made as a check on the hovering points obtained in the vertical-descent runs.

At the larger rates of power-on descent the thrust and torque fluctuated in an irregular manner. An attempt was made in each such case to read the average values.

A chordwise bending fatigue failure occurred on one of the twisted blades while operating at $C_T = 0.004$ at 1600 revolutions per minute and a large rate of power-on descent. Thus the hovering check run was not obtained on these blades.

As previously mentioned, a certain difficulty was experienced in obtaining the reference blade angle for zero thrust. Each of the following available methods appeared likely to introduce certain errors:

1. Assuming the thrust was zero when the calibrated blade angle at the three-quarter-radius point was zero (for untwisted blades)

2. Assuming the calibrated zero point of the thrust strain-gage setup was the same with the rotor stationary and rotating

3. Assuming the thrust was zero when the tufts on the wires in the vicinity of the rotor were undisturbed (for untwisted blades)

In the first case, inaccuracies in the construction of the blades and subsequent warpage due to operating stresses were likely to introduce appreciable error. In the second case, the accuracy is uncertain because of the impossibility of checking the zero-thrust calibration

point on the rotating rotor with the blades installed. Although the calibration factor on the thrust strain-gage spider remained constant during the period of the tests, there were many small zero shifts. Because of the low slope of the hovering values of C_T against θ near the zero-thrust point, the small zero shifts in the thrust could have been translated into appreciable changes in the zero-thrust blade angle. In the third case, induced velocities of the order of ±2 feet per second or less, equivalent to a zero-thrust blade-angle shift of approximately ±0.6° on the 2-foot-radius rotor at 1200 revolutions per minute, could not be detected by the tufts.

In general, method two was assumed to give the correct result unless shown to be obviously in error by method one or three.

REDUCTION OF DATA

In order to present the final data in useful form, it was necessary to determine the operating blade angle at the three-quarter-radius point on the rotating rotors. As previously mentioned, the blades had a symmetrical airfoil section and were designed so that the blade-element elastic axes and aerodynamic centers were very nearly coincident. Also, the calculated chordwise deflections of the blades under the applied torques were very small. Therefore, the theoretical twist due to the air forces acting on the blades should have been negligible and it was thus assumed that the only torque acting to twist the blades was that arising from the inclination of the principal axis of inertia of the blade sections to the plane of rotation.

The resulting dynamic torque was calculated as a function of the blade angle and rotor angular velocity for several stations along a blade for each of the rotors. The spring constants of each blade were then measured experimentally (at three stations on the tapered blades), and the spring constants were averaged for the blades in any given rotor. The dynamic twist between the hub and the three-quarter-radius point was then calculated using the calculated dynamic-torque-loading curve and the experimentally determined spring-constant curve. Over the range of blade angles of these tests the dynamic twist was very nearly a linear function of the blade angle, and the operating blade angle at the three-quarter radius $\theta_{0.75R}$ for the various rotors was given with sufficient accuracy by the expressions:

$$\theta_{0.75R} = 0.820\theta_{root} \text{ at 1600 revolutions per minute}$$

$$\theta_{0.75R} = 0.890\theta_{root} \text{ at 1200 revolutions per minute}$$

for the 6-foot-diameter rotor with constant-chord, untwisted blades,

$$\theta_{0.75R} = 0.963\theta_{root} \text{ at 1600 revolutions per minute}$$

$$\theta_{0.75R} = 0.978\theta_{root} \text{ at 1200 revolutions per minute}$$

for the 4-foot-diameter rotor with constant-chord, untwisted blades,

$$\theta_{0.75R} = 0.940\theta_{root} \text{ at 1600 revolutions per minute}$$

$$\theta_{0.75R} = 0.965\theta_{root} \text{ at 1200 revolutions per minute}$$

for the rotor with untwisted tapered blades, and

$$\theta_{0.75R} = 0.936\left(\theta_{root} - 7.79\right) \text{ at 1600 revolutions per minute}$$

$$\theta_{0.75R} = 0.964\left(\theta_{root} - 7.79\right) \text{ at 1200 revolutions per minute}$$

for the rotor with twisted constant-chord blades. The deflections of the pitch-change linkage were negligible.

The operating blade angle at the three-quarter-radius point was thus found by subtracting the blade pitch-counter reading for zero thrust and zero rate of descent from the blade pitch-counter reading for the test point in question, reading the equivalent blade root angle from the calibration curve, and converting this root angle to the value at the three-quarter-radius point by means of the appropriate equation above.

As a result of the dynamic twist, the actual twist of the rotating blade was slightly different for each test point. However, all comparisons have been made on the basis of the initial static blade twist.

The equivalent free-stream descent velocity was obtained from the calibration curve of wind-tunnel jet velocity against wind-tunnel propeller speed, as explained in the section "Analysis and Discussion."

In the absence of any applicable theory for, or useful measurements of, the radial distribution of the induced velocity for the flight range covered in these tests, it was necessary to make the assumption that the induced velocity was uniform over the rotor in order to obtain the values of λ_i against λ_z or $1/f$ against $1/F$ from the test data.

As a result of this necessary supposition it followed from the assumed geometry that it was a good approximation to take the inflow angle $\emptyset$ as a small angle and consider all blade elements as unstalled. Thus the thrust could be written as

$$T = \frac{1}{2} \rho b c \Omega^2 r^2 c_l \, dr \tag{1}$$

and the torque, as

$$Q = \frac{1}{2} \rho b c \Omega^2 r^3 \left(c_{d_o} - c_l \emptyset \right) dr \tag{2}$$

Then, for a linear twist where the blade angle θ at nondimensional radius $x = r/R$ was given by the expression

$$\theta = \theta_o + \theta_1 x \tag{3}$$

and for an arbitrary plan form denoted by the solidity factors

$$\sigma_1 = \frac{b}{\pi R^2} \int_0^R c \, dr \tag{4}$$

$$\sigma_2 = \frac{b}{\pi R^3} \int_0^R c r \, dr \tag{5}$$

$$\sigma_3 = \frac{b}{\pi R^4} \int_0^R c r^2 \, dr \tag{6}$$

and so forth, the equation used to calculate λ_i from the test values of the thrust coefficient, blade angle, and rate of descent reduced to

$$\lambda_i = \frac{\theta_o \sigma_3 + \theta_1 \sigma_4 - \dfrac{2 C_T}{a}}{\sigma_2 \sqrt{\dfrac{1}{2} \, C_T}} + \lambda_z \tag{7}$$

where

$$\lambda_z = \frac{V}{\Omega R \sqrt{\frac{1}{2} C_T}}$$

$$= \text{Nondimensional velocity of descent} \tag{8}$$

$$\lambda_i = \frac{V_i}{\Omega R \sqrt{\frac{1}{2} C_T}}$$

$$= \text{Nondimensional induced velocity} \tag{9}$$

and a is the two-dimensional lift-curve slope corrected for the Reynolds number and Mach number at the three-quarter-radius point.

Similarly, upon writing the variation of the profile drag coefficient Δc_{d_o} for the symmetrical airfoils as

$$\Delta c_{d_o} = \delta_2 \alpha_r^2 \tag{10}$$

where α_r is the blade-element angle of attack, the solution of the torque equation for λ_i gave

$$\lambda_i = \frac{\left(\dfrac{2\delta_2 - a}{\delta_2 - a}\right)\left(\dfrac{\theta_o \sigma_3 + \theta_1 \sigma_4}{2\sigma_2}\right)}{\sqrt{\dfrac{1}{2} C_T}} + \lambda_z \pm$$

$$\frac{\sqrt{\left(\dfrac{2\delta_2 - a}{\delta_2 - a}\right)^2 \left(\dfrac{\theta_o \sigma_3 + \theta_1 \sigma_4}{2\sigma_2}\right)^2 - \dfrac{\delta_2\left(\theta_o^2 \sigma_4 + \theta_1^2 \sigma_5 + 2\theta_o \theta_1 \sigma_5\right) - 2\Delta C_Q}{\sigma_2\left(\delta_2 - a\right)}}}{\sqrt{\dfrac{1}{2} C_T}}$$

$$\tag{11}$$

where ΔC_Q is the value of C_Q for the test point minus the value at zero thrust and zero rate of descent (i.e., minus the value due to minimum profile drag coefficient).

The Reynolds numbers and Mach numbers at the three-quarter-radius points and the corresponding estimated values of the lift-curve slope used to calculate the values of λ_i are given for each run in tables I to VIII. A value of $\delta_2 = 1.25$ was used to reduce the data, as explained in the section "Analysis and Discussion."

The values of $1/f$ and $1/F$ for the comparison were obtained from the conversion formulas

$$\frac{1}{f} = \lambda_z^2 \tag{12}$$

and

$$\frac{1}{F} = \left(\lambda_i - \lambda_z\right)^2 \tag{13}$$

It is to be noted that the radical of equation (11) may go imaginary if, through experimental errors, the measured torque coefficient ΔC_Q is too large for the measured extended blade root angle θ_o. This was the case for those test points listed in the tables where the value of ΔC_Q is given but the value of λ_i (torque) is missing.

RESULTS

The results of the force tests on each rotor are presented in the form of graphs of $\theta_{0.75R}$ and ΔC_Q against $V/\Omega R$ for constant values of C_T/σ_e and as graphs of the equivalent values of λ_i against λ_z. The experimental values for the individual test points are given in tables I to VIII.

Figures 4, 5, 6, and 7 show the values of $\theta_{0.75R}$ against $V/\Omega R$ at constant C_T/σ_e for the 6-foot-diameter rotors having constant-chord, untwisted blades; tapered blades; and twisted blades; and for the 4-foot-diameter rotor with constant-chord, untwisted blades, respectively. Figures 8, 9, 10, and 11, respectively, show the variation of ΔC_Q with $V/\Omega R$ at constant C_T/σ_e for the four rotors. Figures 12, 13, 14, and 15 show the variation of λ_i with λ_z as calculated for the four rotors from the previous test points.

Figures 16 and 17 show the comparison on λ_i against λ_z and $1/f$ against $1/F$ coordinates of the experimental values obtained from the

data on the 6-foot-diameter rotor having constant-chord, untwisted
blades with the values from Glauert's empirical curve of 1/f against
1/F from reference 1; the full-scale values of references 2 to 4; and
the values given by the simple momentum theory.

Sketches of the flow patterns deduced from the photographs of the
tufts and smoke streamers are shown for values of the nondimensional
descent velocity λ_z of 0, 0.3, 1.0, 1.35, 1.7, and 2.0, respectively,
in figures 18 to 23. Figure 24 shows one of the original smoke photo-
graphs taken at λ_z = 0.3.

The comparison of the theoretical and experimental hovering values
of C_T against $\theta_{0.75R}$ with the values from the end points of the
vertical-descent tests are given in figures 25 to 27. Figures 28 to 30
show the similar comparison for the values of ΔC_Q against C_T.

ANALYSIS AND DISCUSSION

Simple momentum considerations.- Consider the case of an actuator
disk of area A exerting a thrust T and descending at a velocity V
in a perfect fluid. For this hypothetical case there is no apparent
reason why a normal wake should not exist with a flow pattern of the
type shown in figure 31. Consequently, it would appear that the simple
momentum theory could be used to determine the relation between T, V,
and the induced velocity with respect to fixed coordinates V_i. Upon
applying the usual momentum and energy relations it is found that

$$V_i = \frac{V}{2} + \sqrt{\frac{V}{2} + \frac{T}{2\rho A}} \tag{14}$$

and, since

$$\lambda_z = \frac{V}{\sqrt{\dfrac{T}{2\rho A}}}$$

and

$$\lambda_i = \frac{V_i}{\sqrt{\dfrac{T}{2\rho A}}}$$

it follows that

$$\lambda_i = \frac{\lambda_z}{2} + \sqrt{\left(\frac{\lambda_z}{2}\right)^2 + 1} \qquad (15)$$

The values of λ_i given by the above equation might reasonably be expected to constitute a lower limit on the values that can be obtained on an actual rotor for those vertical-descent conditions where the air flow through the plane of rotation is predominantly in a downward direction.

Formation of a "vortex ring" type flow pattern.- Consider, as a second approximation, the case of the actuator disk in a slightly viscous fluid. For the hovering flight condition, the principal effect of the fluid viscosity on the wake is to cause the entrapment of air along the periphery of the wake. As a result, the air within the wake is slowed down, and the diameter of a given section of the stream tube enclosing the wake increases with time and distance from the rotor plane. An analysis of the similar phenomena associated with the expansion of a free jet is given in reference 5.

From the standpoint of elementary vortex theory, the actuator-disk wake can be considered to be composed of a close succession of vortex rings of very small strength. The effect of fluid viscosity upon a vortex filament of one of these rings is to cause a continual increase in core diameter with time. Consequently, after a certain increment of time, the strength of the circulation of a filament measured at any given radius from the axis of the vortex will decrease with time, as explained in reference 6. As the impulse of each vortex ring in the wake tends to remain constant, this implies an increase in ring diameter with time or distance from the rotor and a decrease in velocity of the corresponding point of the wake and the velocity of progression of the rings. Thus, if the actuator disk is slowly allowed to descend from the hovering condition, the downward velocity of the axes of the wake vortex rings will, at some distance below the rotor plane, be less than the descent velocity of the disk and the vortex sheet enclosing the wake will be folded back upon itself as shown schematically in figure 32. When the folded-back sheet has passed above the rotor plane the induced velocities are in such a direction as to cause it to contract and roll up into the "vortex ring" type flow pattern observed at small rates of descent.

For steady-state descent, the strength of the "bound vortex ring" formed by the rolling up of the wake vortex sheet cannot increase with time. Therefore, the vorticity continually shed from the rotor and entering the "bound vortex ring" must leave at the same rate as it enters. Turbulent air exchange between the flow in the ring and the surrounding free-stream flow appears to be the balancing factor.

At the small rates of descent the scale of the turbulence, that is, the volume of the individual masses of air torn from the "bound vortex ring," appears to be small. As the steady-state rate of descent is increased, the scale of the turbulence grows until, at the higher rates of power-on descent, the turbulence becomes severe enough to cause fluctuations in the rotor forces and moments.

Determination of equivalent free-stream velocity.- Upon investigation it appeared that the open-jet method of testing should duplicate the free-stream flow patterns in the vicinity of the rotor with sufficient accuracy but that the measured wind-tunnel velocity would be a poor indication of the equivalent free-stream velocity. For example, at the hovering end points of the tests where the model rotor wake was directed back into the entrance cone of the tunnel, the net tunnel flow corresponding to the free-flight hovering condition would obviously be some small flow in a reversed direction and not a net wind-tunnel flow equal to the zero value of the free-stream rate of descent. For the hovering condition the correct tunnel flow would appear to be that which would occur through the equivalent circle of the tunnel exit cone "above" the rotor in free flight. The magnitude of this flow is not very amenable to calculation. However, it may be noted that this is the quantity of air that would be induced to flow through the wind tunnel by the static-pressure field about the model rotor if the energy ratio of each stream tube passing through the rotor and traversing the circuit of the tunnel were unity, that is, if all the kinetic energy of the fluid in the stream tubes leaving the rotor were dissipated in traversing the circuit of the wind tunnel. A similar situation occurs for the vertical-descent test points except that, for these conditions, there is at present no way of calculating the velocity correction from existing vortex theory.

In the search for some method of obtaining the equivalent free-stream descent velocities from measurable test data, the following method of directly measuring the approximate equivalent free-stream velocity was found and used to reduce the data obtained from the present tests. The method may perhaps be best explained by an analogy.

An open-jet, closed-return wind tunnel with an energy ratio of unity is equivalent aerodynamically to a frictionless open-return tunnel of the type shown in figure 33. For this hypothetical tunnel and, consequently, by analogy, the open-jet, closed-return tunnel having an energy ratio of unity, the total head in a stream tube entering the jet is equal to the atmospheric pressure plus the pressure rise through the plane of the wind-tunnel fan. This is true for the hypothetical open-return tunnel regardless of the changes in tunnel velocity or tunnel velocity distribution caused by the model rotor thrust. Therefore, if, as it seems reasonable to believe, the free-stream static-pressure field about the model is approximately duplicated by the open-jet method of

testing, the velocity distribution about the model in the open jet will be very nearly the same as that of the model in the free stream when the pressure rise through the plane of the wind-tunnel fan is equal to the free-stream velocity head. This can be demonstrated for the case of the hypothetical open-return tunnel by writing Bernoulli's equation along an entering stream tube.

The analogy between the hypothetical frictionless open-return tunnel and the actual closed-return tunnel having an energy ratio of unity is only exact when the pressure drop along each stream tube traversing a circuit of the tunnel is equal to the velocity head of that stream tube as it leaves the tunnel jet. Obviously this requirement can only be satisfied for the particular case where the velocity distribution of the air leaving the tunnel jet is uniform. For the stream tubes originating in the wake of a hovering rotor or a rotor at a very small rate of descent, the diffusion of the rotor wake within the tunnel results in an energy ratio for these stream tubes that is higher than that for the tunnel as a whole. However, the net tunnel flow is in a reverse direction for hovering and for the very small rates of descent at which a jet-type wake exists, and, consequently, the tunnel energy ratio is lower than it is for the higher rates of descent where the flow is in the normal direction. This tends to compensate for the diffusion of the wake in the tunnel.

As a compromise, the tunnel energy ratio was reduced for the present tests to a value of approximately 0.7 by the installation of an 18- by 18-mesh screen, as previously noted.

It was impractical to measure directly the pressure rise through the plane of the wind-tunnel propeller on account of the very small pressure differences involved. Therefore, a calibration was obtained of the wind-tunnel jet velocity against wind-tunnel propeller speed for zero model rotor thrust. Then, making the approximation that the pressure rise through the plane of the wind-tunnel propeller was unchanged by any change in wind-tunnel velocity due to model rotor thrust, the equivalent free-stream velocity at the measured wind-tunnel propeller speed for a given test point could be obtained from this calibration curve.

On the present tests with the very low tunnel energy ratio the wind-tunnel propeller-blade-element inflow angles were small compared with the blade-element angles of attack. Thus the approximation that the pressure rise through the plane of the wind-tunnel propeller was independent of the changes in the wind-tunnel velocity caused by the model rotor thrust did not introduce any large errors.

As a check on the hovering data obtained from the end points of the vertical-descent tests, additional hovering runs were made with the

tunnel blocked at the wake-diffusion screen. This screen was almost
the circuit of the tunnel "below" the rotor. Thus the virtual ground
plane was at some distance greater than the edge of the tunnel exit
cone, five-sixths of a rotor diameter, "below" the rotor, and the
ground effect was very small though probably measurable in view of the
too perfect agreement with the simple independence of blade-element
theory.

The agreement between the values of the hovering blade angles and
torque coefficients obtained from the end points of the vertical-descent
tests with those obtained from the hovering runs with the tunnel blocked
would indicate that the method used to obtain the equivalent free-stream
velocity was approximately correct in the low velocity range.

The good argeement between the nondimensional rate of descent for
"ideal" autorotation obtained from the tests on the 6-foot-diameter
model rotor with the constant-chord, untwisted blades and the full-scale,
free-flight data of references 2 and 3 would indicate that the method
was also useful for the larger descent velocities.

Discussion of discrepancies between present data and those of
reference 7.- The test data of reference 7, used to determine the "vortex
ring" portion of Glauert's curve of $1/f$ against $1/F$, were obtained
on a 3-foot-diameter, two-bladed, solid-brass model of $2\frac{1}{2}$ inch chord in
a 7- by 7-foot square, closed-jet, indraft tunnel. The model blade
angles were adjustable, but not controllable, and runs were obtained at
various set angles up to 6.6° from estimated zero lift. The reference
tunnel velocity was obtained from a static-pressure wall tap located
8 feet ahead of the plane of the test rotor.

The values of $1/F$ calculated from the test data in reference 7
are all too high in the vicinity of hovering because of the use of the
statically set blade angle without any correction for dynamic twist.
For example, the calculated dynamic twist at the three-quarter-radius
point and 1500 revolutions per minute on the model of reference 7 is of
the order of 14 percent of the set root blade angle. If this were to
be taken into account the value of $1/F$ for hovering would be reduced
from 2 to approximately 1.5. The remaining difference between the
residual value of 1.5 and full-scale flight-test values of the order of
1.1 corresponds to a difference in blade angle of only 1/2° which may
have been partially in the assumed blade angle for zero thrust and
partially attributable to an increase in induced velocity due to the
proximity of the closed jet walls.

The tunnel velocity as measured by the static-pressure wall tap was
used in reference 7 as the descent or ascent velocity of the rotor. As

the tunnel velocity contains an increment of the induced velocity of the rotor, it is higher than the equivalent free-stream velocity in the vertical-ascent range and lower than the equivalent free-stream velocity in vertical-descent range. Thus, it could be reasoned that the values of $1/f$ given by Glauert's curve are too high in the vertical-ascent range and too low in the vertical-descent range if they were plotted at the correct values of $1/F$. The loop in the original data of reference 7 at the hovering point would appear to be due to the change in sign of the corrections that would have had to be applied to the measured tunnel velocity in order to obtain the equivalent free-stream velocity.

Calculation of full-scale blade angle and torque coefficient for given thrust coefficient and rate of descent from experimental curves of λ_i against λ_z.- The customary assumption of the independence of blade elements in calculating the thrust and torque of a helicopter rotor in the vertical-descent regime from the experimentally derived values of $1/f$ against $1/F$ or λ_i against λ_z appears to be of doubtful validity to the present authors for two reasons: First, the relations were necessarily calculated from the experimental data on the basis of an assumed uniform normal component of velocity over the rotor disk, and it would seem that the same assumption should be used for inverse computations. Second, that part of the induced flow due to the vortex distribution in the wake will be considerably changed by the large-scale turbulent mixing of the wake air at the higher rates of power-on descent. In other words, the vortex filaments shed from a blade at a given radius probably do not remain at the proportional wake radius long enough for the approximation of the independence of blade elements to be applicable.

Thus, making the same assumptions and approximations that were used to calculate the values of λ_i from the experimental data, namely, that the induced velocity is uniform, the blades are everywhere unstalled, the inflow angle ϕ can be considered a small angle, and the tip loss can be neglected, it follows for blades of given plan form denoted by the solidity factors

$$\sigma_1 = \frac{b}{\pi R^2} \int_0^R c \, dr$$

$$\sigma_2 = \frac{b}{\pi R^3} \int_0^R cr \, dr$$

and so forth and having a linear twist where the blade angle θ at nondimensional radius x is given by the expression $\theta = \theta_o + \theta_1 x$, that the extended root blade angle θ_o is

$$\theta_o = \frac{2C_T}{a\sigma_3} - \sqrt{\frac{1}{2} C_T}\left(\lambda_z - \lambda_i\right)\frac{\sigma_2}{\sigma_3} - \theta_1 \frac{\sigma_4}{\sigma_3} \tag{16}$$

and the torque coefficient is given by the expression

$$C_Q = \frac{1}{2}\delta_o\sigma_4 + \frac{1}{2}\delta_1\left[\theta_o\sigma_4 + \theta_1\sigma_5 + \sqrt{\frac{1}{2}C_T}\left(\lambda_z - \lambda_i\right)\sigma_3\right] +$$

$$\frac{1}{2}\delta_2\left[2\sqrt{\frac{1}{2}C_T}\left(\lambda_z - \lambda_i\right)\left(\theta_o\sigma_3 + \theta_1\sigma_4\right) + \right.$$

$$\left. \frac{1}{2}C_T\left(\lambda_z - \lambda_i\right)^2\sigma_2 + \theta_o{}^2\sigma_4 + \left(2\theta_o + \theta_1\right)\theta_1\sigma_5\right] -$$

$$\frac{1}{2}a\left[\sqrt{\frac{1}{2}C_T}\left(\lambda_z - \lambda_i\right)\left(\theta_o\sigma_3 + \theta_1\sigma_4\right) + \frac{1}{2}C_T\left(\lambda_z - \lambda_i\right)^2\sigma_2\right] \tag{17}$$

The value of λ_i to be used in the above equations is that for the approximate blade taper and twist taken from the appropriate interpolation of the curves of λ_i against λ_z at $\lambda_z = V\left/\Omega R\sqrt{\frac{1}{2}C_T}\right.$. The lift-curve slope a and the coefficients in the equation for the profile drag $c_{d_o} = \delta_o + \delta_1\alpha_r + \delta_2\alpha_r{}^2$, are determined for the blade airfoil at the approximate Reynolds number, Mach number, and surface roughness at the three-quarter-radius point on the blades.

At the higher rates of power-on descent, a certain reduction in the values of λ_i obtained from model tests would appear to be in order for full-scale application as previously noted. However, the considerably lower peak values of λ_i obtained from the flight tests

of reference 2, as shown in figure 16, may have been largely due to the inability, through loss of control, to maintain the desired flight condition long enough for the equilibrium flow to develop. Thus, the magnitude of the correction to be applied is, at present, uncertain and the conservative procedure would be to use the uncorrected model data.

The integrated equations for the hovering values of C_T based on the assumption of the independence of blade elements have not been previously published for the case of rotors having linear taper and twist and thus have been included in an appendix.

Flow patterns.- The recirculation of the air in the "vortex ring" state made it difficult to obtain satisfactory smoke flow pictures. If the smoke streamers were made dense enough to photograph well, the smoke that accumulated in the flow pattern tended to "haze" the picture. If the density of the smoke streamers was reduced, the high turbulence quickly dissipated them. Thus, it was necessary to compromise on a smoke density that showed relatively short lengths of the flow streamlines.

If the tuft studies were to be repeated, it would be desirable to string the wires to which the tufts are attached in a horizontal plane and to take the photographs in a vertical plane. The inclination of the tufts due to gravity could thus be eliminated and the tuft photographs would give a better indication of the flow directions and velocities.

CONCLUDING REMARKS

The mean nondimensional induced velocities calculated from the present test data are considerably less for hovering and very small rates of descent and considerably larger for the higher rates of descent than those given by Glauert's curve of $1/f$ against $1/F$ (where f is the thrust coefficient based on descent velocity and F, the thrust coefficient based on the resultant velocity at the rotor). The major portion of the disagreement can be accounted for and is due to the fact that previously no correction was made for dynamic blade twist and the measured tunnel velocity was taken as the free-stream velocity.

The present data are in good agreement with full-scale flight-test results at the hovering and autorotation ends of the descent range, but the peak values of the nondimensional induced velocity obtained at the large rates of power-on descent are higher than those obtained from the full-scale flight tests reported by Stewart. A part of this discrepancy at the large rates of power-on descent is attributable to the lower

maximum lift coefficient of the model rotor blades, as explained in the discussion. A large part of the remainder may arise from the difficulty, due to loss of control, of maintaining steady-state flight in this region with contemporary helicopters for a long enough period of time for the equilibrium flow to be established.

The primary effects of the 3/1 blade taper were to decrease slightly the mean induced velocity at hovering and the small rates of descent and to increase the "ideal" rate of descent for autorotation by approximately 3 percent over that for the rotor with constant-chord, untwisted blades operating at the same thrust coefficient.

Linear twist of 12° increased the "ideal" nondimensional rate of descent for autorotation by about 10 percent compared with the value for the rotor with the constant-chord, untwisted blades. The peak value of the mean nondimensional induced velocity was increased approximately 24 percent and it occurred at a nondimensional rate of descent that was about 17 percent higher than that for the rotor with the constant-chord, untwisted blades. Also, the fluctuations in the forces and moments on the rotor with the twisted blades were very much larger at the higher rates of power-on descent than for the rotors with the tapered or constant-chord, untwisted blades. As in the case of the tapered blades, the mean induced velocity of the rotor with the twisted blades was slightly less, at hovering, than that for the rotor with the constant-chord, untwisted blades.

There were no observable fluctuations in forces or moments on any of the rotors in the autorotation range.

Within the range and accuracy of these tests there were no significant differences in the curves of nondimensional induced velocity, λ_i against the nondimensional descent velocity λ_z due to variations in the thrust coefficient, rotor speed, or rotor diameter.

The present data should be more applicable to full-scale, free-flight calculations than the data from previous model rotor, vertical-descent tests on account of the inclusion of a correction for the dynamic blade twist and the more exact method used to determine the equivalent free-stream descent velocity.

Georgia Institute of Technology
   Atlanta, Ga., May 31, 1950

APPENDIX

INTEGRATED THRUST EQUATIONS FOR HOVERING ROTORS WITH

LINEARLY TAPERED AND/OR TWISTED BLADES

Assuming independence of blade elements and neglecting the rotation of the slipstream, it follows from the momentum theory that the thrust dT at radius r can be expressed as

$$dT = 4\pi\rho V_i^2 r\, dr \tag{A1}$$

Also, upon making the approximation that the inflow angle ϕ is a small angle, blade-element analysis gives

$$dT = \frac{1}{2}\rho bc\Omega^2 c_l r^2\, dr \tag{A2}$$

Thus, for rotors having blades with a linear taper where the chord c at nondimensional radius x can be denoted in terms of the extended blade root chord c_0 and the taper factor t by the expression

$$c = c_0(1 + tx) \tag{A3}$$

the inflow angle ϕ is

$$\phi = \frac{-V_i}{\Omega r} = -\sqrt{\frac{\sigma_0 c_l(1 + tx)}{8x}} \tag{A4}$$

where $\sigma_0 = \dfrac{bc_0}{\pi R}$, the solidity of the extended blade root chord. However, from the geometry

$$\phi = -\theta + \frac{c_l}{a} \tag{A5}$$

or, for rotors having blades with a linear twist where the blade angle θ at nondimensional radius x can be expressed in terms of the extended blade root pitch angle θ_0 and the twist θ_1 as

$$\theta = \theta_0 + \theta_1 x \tag{A6}$$

it follows that

$$\frac{c_l}{a} = \theta_0 + \theta_1 x + \frac{a\sigma_0}{16}\left(\frac{1 + tx}{x}\right)\left[1 - \sqrt{1 + \frac{32\left(\theta_0 + \theta_1 x\right)x}{a\sigma_0(1 + tx)}}\right] \qquad (A7)$$

This expression can, for convenience, be factored, giving

$$\frac{16c_l}{a^2\sigma_0} = \theta_0 + \theta_1 x + \left(\frac{1 + tx}{x}\right)\left[1 - \sqrt{1 + \frac{2\left(\theta_0 + \theta_1 x\right)x}{1 + tx}}\right] \qquad (A8)$$

where

$$\theta_0 = \frac{16\theta_0}{a\sigma_0} \qquad (A9)$$

$$\theta_1 = \frac{16\theta_1}{a\sigma_0} \qquad (A10)$$

Setting up the expression for the thrust coefficient where

$$C_T = \frac{1}{\rho\pi\Omega^2 R^4}\int_0^R \frac{1}{2}\rho bc\Omega^2 c_l r^2\ dr \qquad (A11)$$

and substituting the previous value of c_l given by equation (A7) yields

$$\frac{32C_T}{a^2\sigma_0^2} = \int_0^1 \left[\theta_0\left(1 + tx\right)x^2 + \theta_1\left(1 + tx\right)x^3 + \left(1 + tx\right)^2 x - \right.$$

$$\left. \left(1 + tx\right)^{3/2}x\sqrt{1 + tx + 2\left(\theta_0 + \theta_1 x\right)x}\right]dx \qquad (A12)$$

Integrating the first three terms of equation (A12) and expanding the factor $(1 + tx)^{3/2}$ in the fourth term by means of the binomial theorem give

$$\frac{32 C_T}{a^2 \sigma_o^2} = \theta_o\left(\frac{1}{3} + \frac{t}{4}\right) + \theta_1\left(\frac{1}{4} + \frac{t}{5}\right) + \frac{1}{2} + \frac{2}{3} t + \frac{1}{4} t^2 -$$

$$\int_0^1 \left[\left(1 + \frac{3}{2} tx + \frac{3}{8} t^2 x^2 - \frac{1}{16} t^3 x^3 + \right.\right.$$

$$\left.\left. \frac{3}{128} t^4 x^4 + \cdots\right) x \sqrt{1 + (2\theta_o + t)x + 2\theta_1 x^2}\right] dx \qquad (A13)$$

Integrating the expansion gives

$$\frac{32 C_T}{a^2 \sigma_o^2} = \theta_o\left(\frac{1}{3} + \frac{t}{4}\right) + \theta_1\left(\frac{1}{4} + \frac{t}{5}\right) + \frac{1}{2} + \frac{2}{3} t + \frac{1}{4} t^2 +$$

$$I + II + III + IV + V \qquad (A14)$$

where

$$I = \frac{1}{6\theta_1}(1 - A) + \frac{(2\theta_o + t)}{4\theta_1}(B) \qquad (A15)$$

$$II = t\left[-\frac{3}{16\theta_1}(A) + \frac{15}{32\theta_1}(2\theta_o + t)(I) + \frac{3}{16\theta_1}(B)\right] \qquad (A16)$$

$$III = t^2\left[-\frac{3}{80\theta_1}(A) - \frac{7}{80\theta_1}(2\theta_o + t)\left(\frac{II}{t}\right) - \frac{3}{40\theta_1}(I)\right] \qquad (A17)$$

$$IV = t^3\left[\frac{1}{192\theta_1}(A) + \frac{1}{16\theta_1}(2\theta_o + t)\left(\frac{III}{t^2}\right) + \frac{1}{96\theta_1} \frac{II}{t}\right] \qquad (A18)$$

$$V = t^4\left[-\frac{3}{1792\theta_1}(A) - \frac{33}{224\theta_1}(2\theta_o + t)\left(\frac{IV}{t^3}\right) - \frac{1}{56\theta_1}\left(\frac{III}{t^2}\right)\right] \qquad (A19)$$

$$A = (2\theta_o + 2\theta_1 + t + 1)^{3/2} \qquad (A20)$$

and, for the case of interest where θ_1 is negative,

$$B = \frac{1}{8\theta_1}\left[\left(2\theta_0 + 4\theta_1 + t\right)\left(2\theta_0 + 2\theta_1 + t + 1\right)^{1/2} - 2\theta_0 - t\right] +$$

$$\frac{\left(2\theta_0 + t\right)^2 - 8\theta_1}{16\theta_1\sqrt{-2\theta_1}}\left\{\sin^{-1}\frac{2\theta_0 + 4\theta_1 + t}{\left[\left(2\theta_0 + t\right)^2 - 8\theta_1\right]^{1/2}} - \right.$$

$$\left. \sin^{-1}\frac{2\theta_0 + t}{\left[\left(2\theta_0 + t\right)^2 - 8\theta_1\right]^{1/2}}\right\} \qquad (A21)$$

It is to be noted that the angles in the above equation are in the first or fourth quadrant depending upon whether the arc sine is positive or negative.

The maximum error introduced in the value of C_T because the sixth and higher terms of the binomial expansion were dropped is less than 1/2 percent for the extreme case where $\theta_1 = -0.2$ radian and $t = -2/3$.

For $\theta_1 = 0$ the latter terms of equation (A14) become imaginary. Thus for tapered but untwisted blades it is necessary to set $\theta_1 = 0$ before integrating. Then for tapered but untwisted blades

$$\frac{32C_T}{a^2\sigma_0^2} = \theta_0\left(\frac{1}{3} + \frac{t}{4}\right) + \frac{1}{2} + \frac{2}{3}t + \frac{1}{4}t^2 + I_1 + II_1 \qquad (A22)$$

where

$$I_1 = -\frac{1}{3t\left(2\theta_0 + t\right)}\left(A_1\right) + \frac{1}{3t\left(2\theta_0 + t\right)} + \frac{\left(\theta_0 + t\right)}{t\left(2\theta_0 + t\right)}\left(B_1\right) \qquad (A23)$$

$$II_1 = -\frac{1}{4\left(2\theta_0 + t\right)}\left(A_1\right) - \frac{5\left(\theta_0 + t\right)}{4\left(2\theta_0 + t\right)}\left(I_1\right) + \frac{1}{4\left(2\theta_0 + t\right)}\left(B_1\right) \qquad (A24)$$

$$A_1 = \left[t(2\theta_o + t) + 2(\theta_o + t) + 1 \right]^{3/2} \tag{A25}$$

and

$$B_1 = \frac{1}{2t(2\theta_o + t)} \left[t(2\theta_o + t) + \theta_o + t \right] \left[t(2\theta_o + t) + \right.$$

$$\left. 2(\theta_o + t) + 1 \right]^{1/2} - \frac{\theta_o + t}{2t(2\theta_o + t)} +$$

$$\frac{\theta_o^2}{2t(2\theta_o + t)\sqrt{-t(2\theta_o + t)}} \left[\sin^{-1} \frac{t(2\theta_o + t) + \theta_o + t}{\theta_o} - \sin^{-1} \frac{\theta_o + t}{\theta_o} \right]$$

$$\tag{A26}$$

For $t = 0$, the latter terms of equation (A22) go imaginary. Thus, for constant-chord, untwisted blades it is necessary to set $t = 0$ before integrating. Then for constant-chord, untwisted blades

$$\frac{32C_T}{a^2\sigma_o^2} = \frac{\theta_o}{3} + \frac{1}{2} + \frac{\left(1 - 3\theta_o\right)\left(1 + 2\theta_o\right)^{3/2} - 1}{15\theta_o^2} \tag{A27}$$

The normal procedure, in using the previous equations which eliminate most of the labor involved in the customary trial-and-error solution for the radial distribution of c_l, is as follows for the usual case where it is desired to take tip loss into account:

1. Calculated R_e, the effective radius, where $R_e = R - \frac{1}{2}$ tip chord.

2. Calculate $\sigma_o = bc_o/\pi R_e$, $C_T' = T/\rho\pi\Omega^2 R_e^4$, and the factor $32C_T'/a^2\sigma_o^2$.

3. Calculate the values of $\theta_1 = 16\theta_1/a\sigma_o$ and $t = \frac{c_{tip}}{c_o} - 1$.

4. Calculate the values of $\theta_O = 16\theta_O/a\sigma_O$ for several assumed
values of θ_O likely to be in the vicinity of and to bridge the value
which will yield the desired thrust coefficient.

5. Calculate the values of $32C_T'/a^2\sigma_O^2$ for the assumed values
of θ_O and the known values of θ_1 and t from the appropriate
equation, (A14), (A22), or (A27).

6. Plot the calculated values of $32C_T'/a^2\sigma_O^2$ against the assumed
values of θ_O and determine the value of θ_O giving the desired value
of $32C_T'/a^2\sigma_O^2$, and, thus, the value of the extended blade root
angle θ_O giving the desired thrust coefficient.

7. Calculate the radial distribution of c_l/a, $\emptyset$, and c_{d_O}, from
equations (A7), (A4), and the airfoil profile drag polar.

8. Obtain the value of C_Q', based on the effective radius, by
graphical integration where

$$C_Q' = -\int_0^1 \frac{1}{2}\sigma_O(1 + tx)c_l\emptyset x^3 \, dx + \int_0^{X'} \frac{1}{2}\sigma_O(1 + tx)c_{d_O}x^3 \, dx$$

and $X' = R/R_e$. The value of c_{d_O} existing at $x = 1$ can be assumed
to extend to X'.

9. Calculate the value of the torque coefficient

$$C_Q = C_Q'\left(\frac{R_e}{R}\right)^5$$

If the radial distributions of the blade air loads are desired,
they can be calculated in the usual manner from the results of item 7
above.

REFERENCES

1. Glauert, H.: The Analysis of Experimental Results in the Windmill
   Brake and Vortex Ring States of an Airscrew. R. & M. No. 1026,
   British A.R.C., 1926.

2. Stewart, W.: Flight Testing of Helicopters. Jour. R.A.S., vol. 52,
   no. 449, May 1948, pp. 261-292; discussion, pp. 293-304.

3. Gessow, Alfred: Flight Investigation of Effects of Rotor-Blade
   Twist on Helicopter Performance in the High-Speed and Vertical-
   Autorotative-Descent Conditions. NACA TN 1666, 1948.

4. Gustafson, F. B., and Gessow, Alfred: Flight Tests of the Sikorsky
   HNS-1 (Army YR-4B) Helicopter. II - Hovering and Vertical-Flight
   Performance with the Original and an Alternate Set of Main-Rotor
   Blades, Including a Comparison with Hovering Performance Theory.
   NACA MR L5D09a, 1945.

5. Prandtl, L.: The Mechanics of Viscous Fluids. Spread of Turbulence.
   Vol. III of Aerodynamic Theory, div. G, sec. 25, W. F. Durand, ed.,
   Julius Springer (Berlin), 1935, pp. 172-173.

6. Prandtl, L.: The Mechanics of Viscous Fluids. Some Examples of
   Exact Solutions. Vol. III of Aerodynamic Theory, div. G, sec. 10,
   W. F. Durand, ed., Julius Springer (Berlin), 1935, pp. 68-69.

7. Lock, C. N. H., Bateman, H., and Townend, H. C. H.: An Extension
   of the Vortex Theory of Airscrews with Applications to Airscrews
   of Small Pitch, Including Experimental Results. R. & M. No. 1014,
   British A.R.C., 1926.

TABLE I.- SUMMARY OF DATA ON 6-FOOT-DIAMETER ROTOR WITH CONSTANT-CHORD, UNTWISTED BLADES

$V/\Omega R$	$\theta_{0.75R}$	ΔC_Q	λ_z	λ_1 (thrust)	λ_1 (torque)	$V/\Omega R$	$\theta_{0.75R}$	ΔC_Q	λ_z	λ_1 (thrust)	λ_1 (torque)
Run 3; $C_T = 0.004$; 1200 rpm						Run 32; $C_T = 0.002$; 1200 rpm					
0	8.83	0.000282	0	1.10	----	0	5.32	0.000087	0	0.97	1.09
.0400	8.74	.000249	.91	1.98	2.08	.0048	5.00	.000087	.15	1.01	1.05
.0556	8.83	.000251	1.27	2.37	2.48	.0161	5.21	.000077	.50	1.43	1.67
.0658	8.83	.000266	1.50	2.60	2.47	.0298	4.91	.000075	.92	1.75	1.91
.0799	4.10	.000009	1.83	1.69	1.53	.0376	5.00	.000080	1.15	2.01	2.12
.0762	4.87	.000039	1.74	1.81	1.57	.0442	5.22	.000086	1.36	2.30	2.39
.0795	3.99	.000010	1.82	1.65	1.54	.0484	5.22	.000087	1.49	2.42	2.49
Run 4; $C_T = 0.004$; 1200 rpm						.0552	1.90	.000007	1.70	1.47	1.65
						.0592	1.39	-.000002	1.82	1.42	1.64
0	8.66	0.000285	0	1.05	----	.0641	.42	-.000025	1.97	1.22	1.39
.0168	8.40	.000270	.38	1.37	----	.0676	-.28	-.000042	2.08	1.09	1.24
.0254	8.49	.000262	.58	1.59	----	.0721	-.84	-.000092	2.21	1.03	.90
.0400	8.32	.000243	.91	1.87	----	.0771	-1.46	-.000069	2.37	.97	1.10
.0550	8.37	.000239	1.26	2.23	2.19	Run 34; $C_T = 0.002$; 1600 rpm					
.0649	8.54	.000256	1.48	2.50	----						
.0702	7.24	.000177	1.61	2.29	2.45	0	5.33	0.000087	0	1.13	1.16
.0734	4.79	.000046	1.67	1.72	1.57	.0043	5.12	.000083	.36	1.41	1.43
.0790	4.10	.000018	1.81	1.67	1.57	.0113	5.12	.000084	.61	1.66	1.67
.0859	2.87	-.000024	1.96	1.51	1.53	.0191	4.81	.000073	.91	1.84	1.92
.0949	1.23	-.000112	2.17	1.29	1.23	.0282	4.90	.000077	1.13	2.10	2.13
Run 5; $C_T = 0.004$; 1200 rpm						.0350	5.22	.000080	1.27	2.36	2.48
						.0395	5.21	.000082	1.43	2.51	2.60
0	8.86	0.000292	0	1.10	----	.0444	3.89	.000065	1.55	2.15	----
.0176	8.70	.000279	.40	1.47	----	.0481	3.89	.000055	1.63	2.22	----
.0265	8.53	.000270	.60	1.62	----	.0504	1.88	.000006	1.72	1.58	1.65
.0388	8.40	.000245	.89	1.87	----	.0533	1.35	-.000007	1.84	1.51	1.55
.0552	8.53	.000249	1.26	2.28	----	.0572	.55	-.000028	2.01	1.38	1.39
.0617	8.48	.000256	1.41	2.42	----	.0624	-.30	-.000053	2.22	1.28	1.24
.0670	8.46	.000250	1.53	2.53	----	.0690	-.77	-.000078	2.39	1.28	1.14
.0734	4.60	.000039	1.67	1.67	----	Run 35; $C_T = 0.004$; 1600 rpm					
.0790	3.99	.000011	1.81	1.64	----						
.0856	2.58	-.000039	1.96	1.43	----	0	8.68	0.000271	0	1.08	----
.0949	1.18	-.000116	2.17	1.27	----	.0098	8.64	.000270	.22	1.29	----
Run 6; $C_T = 0.002$; 1200 rpm						.0162	8.50	.000261	.37	1.40	----
						.0215	8.50	.000261	.49	1.52	----
0	5.33	--------	0	1.11	----	.0295	8.45	.000248	.67	1.69	1.61
.0190	4.95	--------	.61	1.58	----	.0411	8.30	.000234	.94	1.92	1.98
.0300	4.75	--------	.97	1.87	----	.0485	8.30	.000229	1.10	2.09	2.22
.0382	4.92	--------	1.23	2.19	----	.0513	8.30	.000229	1.17	2.15	2.28
.0447	5.16	--------	1.44	2.49	----	.0566	8.30	.000239	1.29	2.27	2.22
.0490	4.26	--------	1.58	2.30	----	.0624	8.30	.000243	1.42	2.41	----
.0556	1.44	--------	1.80	1.48	----	.0684	7.22	.000175	1.56	2.26	2.50
.0596	.56	--------	1.92	1.28	----	.0739	4.36	.000048	1.69	1.64	1.72
Run 9; $C_T = 0.002$; 1600 rpm						.0795	3.67	.000020	1.81	1.59	1.69
						.0835	3.29	.000001	1.91	1.58	1.67
0	5.13	0.000062	0	1.05	1.41	.0381	2.46	-.000045	2.01	1.47	1.50
.0136	5.26	.000072	.43	1.54	1.79	Run 36; $C_T = 0.004$; 1200 rpm					
.0214	4.87	.000067	.69	1.65	1.87						
.0303	4.88	.000065	.98	1.94	2.19	0	8.49	0.000242	0	1.01	1.06
.0373	4.81	.000067	1.20	2.14	2.34	.0066	8.68	.000247	.15	1.21	1.32
.0417	5.03	.000077	1.35	2.36	2.47	.0163	8.82	.000254	.37	1.47	1.57
.0463	5.01	.000081	1.50	2.51	2.53	.0238	8.74	.000245	.54	1.62	1.78
.0501	3.44	.000045	1.62	2.05	----	.0353	8.68	.000232	.81	1.86	2.13
.0525	1.94	.000030	1.69	1.57	1.55	.0459	8.51	.000215	1.05	2.06	2.40
.0561	1.27	-.000002	1.81	1.44	1.63	.0525	8.72	.000224	1.20	2.27	2.61
.0602	.68	-.000028	1.94	1.35	1.33	.0590	8.62	.000233	1.35	2.39	2.61
.0650	-.11	-.000050	2.10	1.22	1.17	.0652	8.80	.000247	1.49	2.58	2.75
.0720	-1.32	-.000072	2.32	1.00	1.00	.0684	8.00	.000194	1.56	2.44	2.80
.0763	-1.66	-.000084	2.46	1.02	.99	.0715	6.34	.000106	1.63	2.08	2.77
Run 14; $C_T = 0.005$; 1600 rpm						.0764	5.25	.000054	1.75	1.91	----
						.0831	4.29	.000016	1.90	1.81	1.67
0	10.06	0.000414	0	1.03	----	.0914	2.81	-.000047	2.09	1.62	1.56
.0103	9.99	.000409	.21	1.21	----	Run 38; $C_T = 0.005$; 1600 rpm					
.0215	9.81	.000400	.43	1.54	----						
.0287	10.02	.000396	.57	1.79	----	0	10.19	--------	0	1.05	----
.0386	10.13	.000397	.77	1.81	----	.0096	10.18	--------	.20	1.24	----
.0510	10.36	--------	1.02	2.11	----	.0161	10.18	--------	.33	1.38	----
.0548	10.69	--------	1.10	2.27	----	.0210	10.02	--------	.43	1.44	----
.0586	10.96	--------	1.17	2.40	----	.0271	10.02	--------	.55	1.56	----
.0656	10.92	--------	1.31	2.54	----	.0364	10.14	--------	.74	1.78	----
.0722	9.80	--------	1.44	2.41	----	.0496	10.41	--------	1.01	2.11	----
.0762	9.80	--------	1.52	2.49	----	.0535	10.22	--------	1.09	2.15	----
.0782	9.79	.000377	1.56	2.53	----	.0569	10.14	--------	1.16	2.20	----
.0818	5.07	.000091	1.64	1.50	----	.0602	10.14	--------	1.23	2.27	----
.0888	5.49	.000086	1.78	1.74	1.89	.0629	9.98	--------	1.28	2.28	----
.0898	4.89	.000051	1.80	1.62	1.75	.0662	9.98	--------	1.35	2.35	----
.0958	3.52	-.000016	1.92	1.42	1.79	.0695	9.84	--------	1.42	2.39	----
0	10.01	.000407	----	----	----	.0745	10.22	--------	1.52	2.58	----
						.0765	9.35	0.000172	1.56	2.42	----
						.0801	6.58	.000146	1.63	1.84	1.98
						.0819	6.45	.000130	1.71	1.89	1.88
						.0883	5.22	.000094	1.80	1.70	2.09
						.0940	4.77	.000038	1.92	1.71	1.77
						.1032	3.39	-.000060	2.11	1.58	1.54

NACA
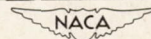
TABLE II.- SUMMARY OF DATA ON 6-FOOT-DIAMETER ROTOR HAVING UNTWISTED BLADES WITH 3/1 TAPER

$V/\Omega R$	$\theta_{0.75R}$	Δc_Q	λ_z	λ_1 (thrust)	λ_1 (torque)
Run 48; $c_T = 0.002$; 1200 rpm					
0	5.40	0.000086	0	1.03	0.98
.0068	5.40	.000085	.22	1.24	1.22
.0188	5.04	.000076	.61	1.50	1.48
.0300	4.81	.000068	.97	1.78	1.82
.0376	4.99	.000075	1.21	2.09	2.06
.0437	5.26	.000081	1.42	2.37	2.36
.0477	4.95	.000074	1.54	2.39	2.36
.0552	3.62	.000052	1.79	2.19	2.19
.0588	1.40	-.000005	1.90	1.56	1.62
.0634	-.13	-.000020	2.05	1.20	1.47
.0669	-.68	-.000037	2.17	1.13	1.31
.0716	-1.53	-.000051	2.32	.99	----
.0771	-2.10	-.000068	2.50	.98	----
.0840	-3.03	-.000083	2.72	.89	----
Run 49; $c_T = 0.004$; 1200 rpm					
0	9.00	0.000248	0	1.01	1.05
.0051	9.00	.000248	.11	1.12	1.17
.0159	9.05	.000245	.36	1.37	1.48
.0241	9.00	.000238	.54	1.55	1.71
.0360	9.00	.000235	.81	1.81	2.00
.0455	9.00	.000229	1.02	2.03	2.27
.0526	9.13	.000238	1.18	2.21	2.42
.0597	8.87	.000229	1.34	2.31	2.52
.0628	9.20	.000239	1.41	2.46	2.66
.0681	9.20	.000243	1.53	2.58	2.77
.0716	7.75	.000179	1.60	2.31	2.71
.0760	6.33	.000122	1.70	2.08	2.16
.0822	3.13	-.000006	1.84	1.47	1.89
.0910	1.02	-.000086	2.04	1.17	1.48
Run 50; $c_T = 0.005$; 1200 rpm					
0	10.73	0.000365	0	1.03	0.92
.0035	10.68	.000367	.07	1.09	----
.0130	11.07	.000395	.27	1.37	----
.0223	11.07	.000398	.46	1.55	----
.0323	10.96	.000387	.66	1.73	----
.0612	10.78	.000366	1.25	2.27	2.21
.0645	10.78	.000368	1.32	2.34	2.23
.0685	10.78	.000368	1.40	2.42	2.31
.0723	10.78	.000369	1.47	2.49	2.35
.0733	9.60	.000302	1.58	2.34	----
.0831	8.48	.000227	1.70	2.23	2.20
.0913	4.15	.000009	1.86	1.48	1.61
.0980	3.02	-.000063	2.00	1.38	1.44
Run 51; $c_T = 0.002$; 1600 rpm					
0	5.40	0.000098	0	1.05	----
.0046	5.16	.000096	.15	1.11	----
.0128	4.79	.000091	.41	1.25	----
.0194	4.79	.000088	.63	1.46	----
.0280	4.79	.000086	.91	1.73	----
.0350	4.69	.000077	1.13	1.92	----
.0398	4.97	.000086	1.29	2.16	----
.0447	5.12	.000091	1.45	2.37	----
.0465	5.12	.000090	1.51	2.43	----
.0485	5.21	.000091	1.57	2.52	----
.0501	4.69	.000085	1.62	2.40	----
.0528	3.31	.000065	1.71	2.03	----
.0561	2.24	.000041	1.82	1.75	----
.0604	-.11	-.000017	1.96	----	1.22
.0674	-1.28	-.000042	2.18	.97	1.14
.0715	-1.91	-.000054	2.32	.89	1.04
Run 54; $c_T = 0.004$; 1600 rpm					
0	8.99	--------	0	1.03	----
.0093	8.99	--------	.21	1.24	----
.0153	8.99	--------	.34	1.37	----
.0191	8.99	--------	.43	1.46	----
.0299	9.14	--------	.68	1.73	----
.0418	9.46	--------	.95	2.07	----
.0495	9.17	--------	1.12	2.18	----
.0524	9.17	--------	1.19	2.24	----
.0558	9.17	--------	1.26	2.32	----
.0583	9.17	--------	1.32	2.38	----
.0617	9.17	--------	1.40	2.45	----
.0652	9.17	--------	1.48	2.53	----
.0684	9.17	--------	1.55	2.60	----
.0755	7.09	--------	1.71	2.27	----
.0797	4.16	--------	1.80	1.68	----
.0830	2.41	--------	1.88	1.34	----
.0875	1.20	--------	1.98	1.16	----

$V/\Omega R$	$\theta_{0.75R}$	Δc_Q	λ_z	λ_1 (thrust)	λ_1 (torque)
Run 58; $c_T = 0.002$; 1200 rpm					
0	5.40	0.000082	0	1.01	1.06
.0053	5.22	.000081	.17	1.12	1.10
.0168	5.00	.000075	.53	1.41	1.40
.0296	5.00	.000068	.95	1.82	1.96
.0371	5.00	.000071	1.19	2.05	2.14
.0429	5.18	.000076	1.37	2.30	2.37
.0472	5.18	.000076	1.51	2.43	2.51
.0539	3.45	.000045	1.73	2.07	2.13
.0574	1.45	.000000	1.84	1.52	1.68
.0618	.60	-.000014	1.98	1.38	1.55
.0650	-.34	-.000030	2.08	1.17	1.42
.0696	-.62	-.000041	2.23	1.22	----
.0767	-1.60	-.000064	2.46	1.12	----
Run 59; $c_T = 0.005$; 1200 rpm					
0	10.78	--------	0	1.04	----
.0048	10.78	--------	.07	1.14	----
.0141	10.47	--------	.27	1.30	----
.0243	10.71	--------	.46	1.52	----
.0360	10.71	--------	.66	1.75	----
.0470	10.81	--------	.92	1.99	----
.0537	10.62	--------	1.11	2.09	----
.0610	10.62	--------	1.25	2.23	----
.0641	10.62	--------	1.32	2.29	----
.0678	10.62	--------	1.40	2.37	----
.0725	10.62	--------	1.47	2.42	----
.0731	10.62	--------	1.55	2.48	----
.0782	9.82	--------	1.58	2.41	----
.0839	8.50	--------	1.70	2.25	----
.0923	5.34	--------	1.86	1.75	----
.0945	3.21	--------	2.00	1.35	----
Run 61; $c_T = 0.002$; 1600 rpm					
0	5.33	0.000095	0	0.99	----
0	5.38	.000100	0	1.00	----
.0036	5.38	.000101	.11	1.12	----
.0116	5.38	.000099	.37	1.37	----
.0179	5.27	.000094	.57	1.53	----
.0269	4.95	.000088	.85	1.71	----
.0349	4.69	.000083	1.10	1.88	----
.0398	4.69	.000085	1.26	2.03	----
.0445	4.69	.000086	1.40	2.18	----
.0471	4.95	.000090	1.49	2.35	----
.0496	5.33	.000095	1.57	2.56	----
.0511	4.41	.000083	1.61	2.30	----
.0541	3.89	.000069	1.71	2.22	----
.0578	2.21	.000038	1.82	1.78	----
.0626	.01	-.000013	1.97	1.20	1.54
.0694	-1.62	-.000040	2.19	.88	1.14
.0740	-2.52	-.000056	2.34	.73	.96
.0797	-3.43	-.000074	2.52	.61	.81
Run 64; $c_T = 0.004$; 1600 rpm					
0	9.01	--------	0	1.09	----
.0038	9.01	--------	.09	1.17	----
.0109	8.86	--------	.25	1.30	----
.0153	9.01	--------	.35	1.42	----
.0201	9.01	--------	.47	1.54	----
.0262	9.03	--------	.61	1.68	----
.0365	9.19	--------	.85	1.95	----
.0473	9.30	--------	1.10	2.21	----
.0504	9.30	--------	1.17	2.28	----
.0534	9.30	--------	1.24	2.35	----
.0566	9.10	--------	1.31	2.37	----
.0601	9.10	--------	1.39	2.45	----
.0637	9.33	--------	1.48	2.59	----
.0677	9.33	--------	1.57	2.68	----
.0722	9.33	--------	1.68	2.78	----
.0743	6.85	--------	1.73	2.24	----
.0785	4.62	--------	1.82	1.82	----
.0820	1.56	--------	1.90	1.18	----
.0865	-.10	--------	2.01	----	----
.0921	-1.18	--------	2.14	----	----

NACA

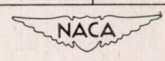## TABLE III.- SUMMARY OF DATA ON 6-FOOT-DIAMETER ROTOR WITH CONSTANT-CHORD, TWISTED BLADES (12° LINEAR WASHOUT)

$V/\Omega R$	$\theta_{0.75R}$	ΔC_Q	λ_z	λ_i (thrust)	λ_i (torque)	$V/\Omega R$	$\theta_{0.75R}$	ΔC_Q	λ_z	λ_i (thrust)	λ_i (torque)
Run 65; C_T = 0.002; 1200 rpm						Run 67; C_T = 0.005; 1200 rpm					
0	4.93	0.000079	0	1.04	1.03	0	10.80	0.000377	0	1.17	0.99
.0066	4.93	.000078	.21	1.25	1.26	.0057	10.66	.000364	.12	1.26	1.29
.0181	4.76	.000074	.59	1.57	1.59	.0152	10.66	.000361	.31	1.45	1.46
.0287	4.52	.000068	.93	1.82	1.88	.0221	10.33	.000332	.45	1.52	1.65
.0364	4.52	.000065	1.18	2.07	2.20	.0305	10.53	.000333	.63	1.74	1.95
.0424	4.69	.000066	1.38	2.33	2.50	.0435	10.13	.000307	.89	1.93	2.19
.0486	4.93	.000076	1.58	2.61	2.67	.0538	10.30	.000301	1.11	2.16	2.53
.0550	5.64	.000090	1.78	3.07	3.15	.0609	10.30	.000296	1.25	2.31	2.71
.0579	5.99	.000101	1.86	3.27	3.29	.0644	10.30	.000308	1.32	2.38	2.70
.0612	4.65	.000078	1.99	2.92	----	.0684	10.66	.000331	1.40	2.54	2.83
.0649	3.63	.000058	2.11	2.68	----	.0713	10.80	.000338	1.46	2.64	2.91
.0702	-.46	-.000021	2.28	1.40	1.54	.0753	11.28	.000366	1.55	2.83	3.06
.0755	-1.85	-.000038	2.45	1.08	1.26	.0806	11.67	.000393	1.65	3.02	3.21
.0819	-2.80	-.000051	2.66	.96	1.13	.0832	10.72	.000350	1.71	2.86	3.01
.0914	-4.20	-.000070	2.97	.77	.94	.0904	6.20	.000149	1.85	1.99	----
.0976	-4.73	-.000081	3.17	.78	.93	.0967	5.41	.000111	1.98	1.95	----
0	5.12	.000085	0	----	----	.1044	3.64	.000053	2.14	1.70	----
						.1094	2.17	-.000028	2.25	1.48	1.86
Run 66; C_T = 0.004; 1200 rpm						0	11.07	.000382	0	1.23	1.26
0	8.67	0.000252	0	1.07	----	Run 68; C_T = 0.002; 1600 rpm					
.0057	8.67	.000251	.13	1.20	----						
.0157	8.67	.000248	.36	1.43	----	0	5.12	0.000083	0	1.05	0.96
.0238	8.34	.000231	.55	1.53	----	.0183	5.03	.000089	.59	1.61	----
.0351	8.52	.000223	.80	1.84	1.98	.0269	4.80	.000080	.87	1.81	----
.0459	8.16	.000208	1.05	2.00	2.15	.0340	4.49	.000072	1.10	1.93	----
.0526	8.16	.000202	1.20	2.15	2.37	.0388	4.21	.000065	1.25	1.99	----
.0594	8.48	.000218	1.36	2.39	2.57	.0440	4.82	.000073	1.42	2.36	2.38
.0627	8.69	.000227	1.44	2.52	2.69	.0466	4.88	.000073	1.50	2.46	2.51
.0669	9.08	.000214	1.53	2.71	3.09	.0492	5.38	.000080	1.58	2.72	2.82
.0698	9.32	.000253	1.60	2.33	2.99	.0518	5.57	.000084	1.67	2.87	2.96
.0733	9.61	.000270	1.68	2.99	3.11	.0546	5.96	.000092	1.76	3.09	3.18
.0763	8.80	.000244	1.75	2.85	2.87	.0570	5.96	.000095	1.84	3.17	3.22
.0816	4.31	.000073	1.87	1.85	----	.0611	3.52	.000068	1.97	2.47	----
.0906	2.40	.000014	2.08	1.58	2.00	.0677	-1.13	-.000020	2.18	1.10	1.34
.0972	1.03	-.000038	2.23	1.38	1.70	.0723	-1.86	-.000034	2.33	1.00	1.20
.1020	-.50	-.000066	2.34	1.11	1.52	.0781	-2.90	-.000049	2.52	.83	1.02
0	8.62	.000249	0	1.06	----	.0821	-3.56	-.000061	2.64	.73	.89
						.0862	-4.15	-.000066	2.78	.67	.84
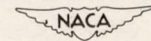
TABLE IV.- SUMMARY OF DATA ON 4-FOOT-DIAMETER ROTOR WITH CONSTANT-CHORD,

UNTWISTED BLADES

$V/\Omega R$	$\theta_{0.75R}$	ΔC_Q	λ_z	λ_i (thrust)	λ_i (torque)
Run 20; $C_T = 0.002$; 1200 rpm					
0	5.06	0.000083	0	1.05	0.95
.0277	5.32	.000056	.88	1.99	2.39
.0377	5.43	.000062	1.19	2.38	2.74
.0400	5.32	.000057	1.27	2.41	2.81
.0491	5.06	.000052	1.56	2.61	3.02
.0597	1.87	-.000013	1.89	1.76	1.48
.0702	-.39	-.000053	2.22	1.27	1.20
.0818	-2.48	-.000079	2.59	.86	.94
Run 22; $C_T = 0.005$; 1200 rpm					
0	9.89	0.000305	0	0.96	1.27
.0099	10.35	.000312	.20	1.26	1.68
.0307	11.08	.000330	.61	1.85	2.33
.0431	10.69	.000312	.86	2.00	2.50
.0531	10.69	.000312	1.06	2.20	2.70
.0627	11.04	.000348	1.25	2.48	2.87
.0691	9.98	.000321	1.28	2.36	2.58
.0824	6.91	.000168	1.65	1.91	----
.0888	6.16	.000136	1.78	1.87	----
.0961	5.09	.000088	1.92	1.76	2.35
.1015	3.36	-.000009	2.03	1.47	1.74
.1068	2.09	-.000083	2.14	1.28	1.48
Run 23; $C_T = 0.002$; 1600 rpm					
0	4.95	0.000089	0	0.95	----
.0092	4.95	.000082	.29	1.24	1.20
.0239	4.99	.000073	.76	1.73	1.90
.0323	5.34	.000083	1.03	2.12	2.27
.0390	5.34	.000084	1.24	2.33	2.47
.0463	4.93	.000072	1.47	2.42	2.58
.0532	3.48	.000042	1.69	2.11	2.16
.0627	.75	-.000011	1.99	1.42	1.64
.0671	-.54	-.000032	2.14	1.09	1.33
.0725	-1.33	-.000058	2.30	.97	1.11
.0765	-2.19	-.000073	2.44	.80	.94
Run 24; $C_T = 0.005$; 1600 rpm					
0	9.99	0.000322	0	0.99	1.28
.0226	10.00	.000298	.46	1.44	1.90
.0335	10.66	.000299	.68	1.81	2.40
.0415	10.48	.000283	.84	1.93	2.55
.0488	10.29	.000270	.99	2.03	2.68
.0630	10.29	.000306	1.28	2.32	2.80
.0720	8.05	.000196	1.46	1.98	1.68
.0761	7.42	.000171	1.54	1.91	1.78
.0813	6.96	.000155	1.64	1.91	1.92
.0865	----	.000135	1.75	----	----
.0935	4.85	.000044	1.90	1.66	1.78
.1040	2.18	-.000101	2.12	1.25	1.38
.1106	.96	-.000167	2.25	1.10	1.22

$V/\Omega R$	$\theta_{0.75R}$	ΔC_Q	λ_z	λ_i (thrust)	λ_i (torque)
Run 25; $C_T = 0.004$; 1600 rpm					
0	8.54	0.000221	0	1.04	1.35
.0239	8.45	.000200	.54	1.55	1.99
.0330	8.70	.000185	.75	1.82	2.39
.0405	8.70	.000192	.92	1.99	2.52
.0480	9.06	.000209	1.09	2.25	2.75
.0551	9.32	.000229	1.26	2.48	2.92
.0625	8.33	.000200	1.43	2.39	2.80
.0666	7.25	.000156	1.53	2.20	2.67
.0720	6.03	.000100	1.64	2.00	1.72
.0757	5.47	.000079	1.73	1.94	1.76
.0810	4.26	.000030	1.85	1.70	1.69
.0863	2.58	-.000027	1.97	1.42	1.53
.0931	.88	-.000098	2.13	1.13	1.25
Run 28; $C_T = 0.004$; 1600 rpm					
0	8.60	0.000236	0	1.06	1.26
.0207	8.79	.000227	.47	1.57	1.91
.0330	8.79	.000208	.75	1.84	2.31
.0411	8.86	.000213	.93	2.05	2.49
.0480	9.29	.000219	1.09	2.31	2.80
.0552	9.41	.000241	1.26	2.50	2.90
.0630	8.43	.000214	1.43	2.42	2.76
.0667	7.43	.000159	1.52	2.24	2.74
Run 30; $C_T = 0.004$; 1200 rpm					
0	8.64	0.000220	0	1.17	1.36
.0112	8.32	--------	.27	1.34	----
.0300	8.32	--------	.73	1.76	----
.0413	8.84	--------	1.01	2.15	----
.0515	9.22	.000199	1.26	2.47	2.91
.0601	8.12	.000182	1.47	2.38	2.72
.0700	5.76	.000070	1.71	1.99	----
.0825	3.12	.000001	2.02	1.58	1.61
.0885	1.12	-.000067	2.16	1.20	1.29
.0950	-.56	-.000117	2.32	.91	1.16

NACA
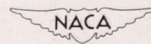
TABLE V.- HOVERING DATA FOR 6-FOOT-DIAMETER ROTOR

WITH CONSTANT-CHORD, UNTWISTED BLADES

$\theta_{0.75R}$	C_T	ΔC_Q
Run 15; 1200 rpm		
0	0	0
1.26	.00028	.000002
3.08	.00098	.000024
4.91	.00168	.000070
6.68	.00289	.000137
8.46	.00400	.000226
10.29	.00488	.000342
11.99	.00526	--------
Run 16; 1600 rpm		
0	0	0
.63	.00013	.000001
2.31	.00075	.000016
3.96	.00160	.000053
5.55	.00255	.000108
7.18	.00346	.000194
8.85	.00421	.000301
Run 39; 1200 rpm		
0	0	0
1.66	.00024	.000006
3.42	.00088	.000029
5.22	.00179	.000070
6.99	.00284	.000138
8.70	.00414	.000228
10.34	.00513	.000323
Run 41; 1600 rpm		
----	0	0
1.53	.00018	.000004
3.15	.00089	.000025
4.81	.00187	.000050
6.45	.00278	.000114
8.02	.00374	.000199
9.53	.00471	.000321

NACA

TABLE VI.- HOVERING DATA FOR 6-FOOT-DIAMETER ROTOR

HAVING UNTWISTED BLADES WITH 3/1 TAPER

$\theta_{0.75R}$	C_T	ΔC_Q
Run 44		
0	0	0
1.15	.00019	.000005
1.20	.00026	.000007
3.00	.00087	.000017
3.02	.00090	.000025
3.12	.00094	.000030
4.90	.00175	.000055
5.07	.00194	.000054
6.78	.00277	.000113
7.00	.00300	.000117
8.64	.00404	.000213
8.86	.00413	.000228
10.65	.00496	.000340

NACA
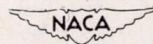
TABLE VII.- HOVERING DATA FOR 4-FOOT-DIAMETER ROTOR

WITH CONSTANT-CHORD, UNTWISTED BLADES

$\theta_{0.75R}$	C_T	ΔC_Q
Run 17; 1200 rpm		
0	0	0
1.11	.00017	.000002
2.10	.00052	.000016
4.05	.00152	.000058
6.02	.00275	.000110
8.00	.00397	.000196
9.92	.00468	.000271
11.73	.00527	.000375
8.30	.00411	.000229
Run 18; 1600 rpm		
0	0	0
1.93	.00044	.000020
3.83	.00136	.000050
5.70	.00245	.000109
7.72	.00382	.000203
9.61	.00477	.000279
11.39	.00535	.000373
7.68	.00379	.000201
3.83	.00135	.000041

NACA
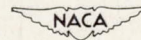
TABLE VIII.- VALUES OF MACH NUMBER, REYNOLDS NUMBER, AND

CALCULATED SLOPE OF LIFT CURVE AT THREE-QUARTER-

RADIUS POINT FOR TEST CONDITIONS

Speed (rpm)	4-foot-diameter rotor			6-foot-diameter rotors		
	Mach number	Reynolds number	Slope of lift curve	Mach number	Reynolds number	Slope of lift curve
1200	0.165	114,000	5.83	0.248	256,000	5.95
1600	.220	152,000	5.90	.330	341,000	6.07
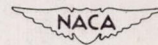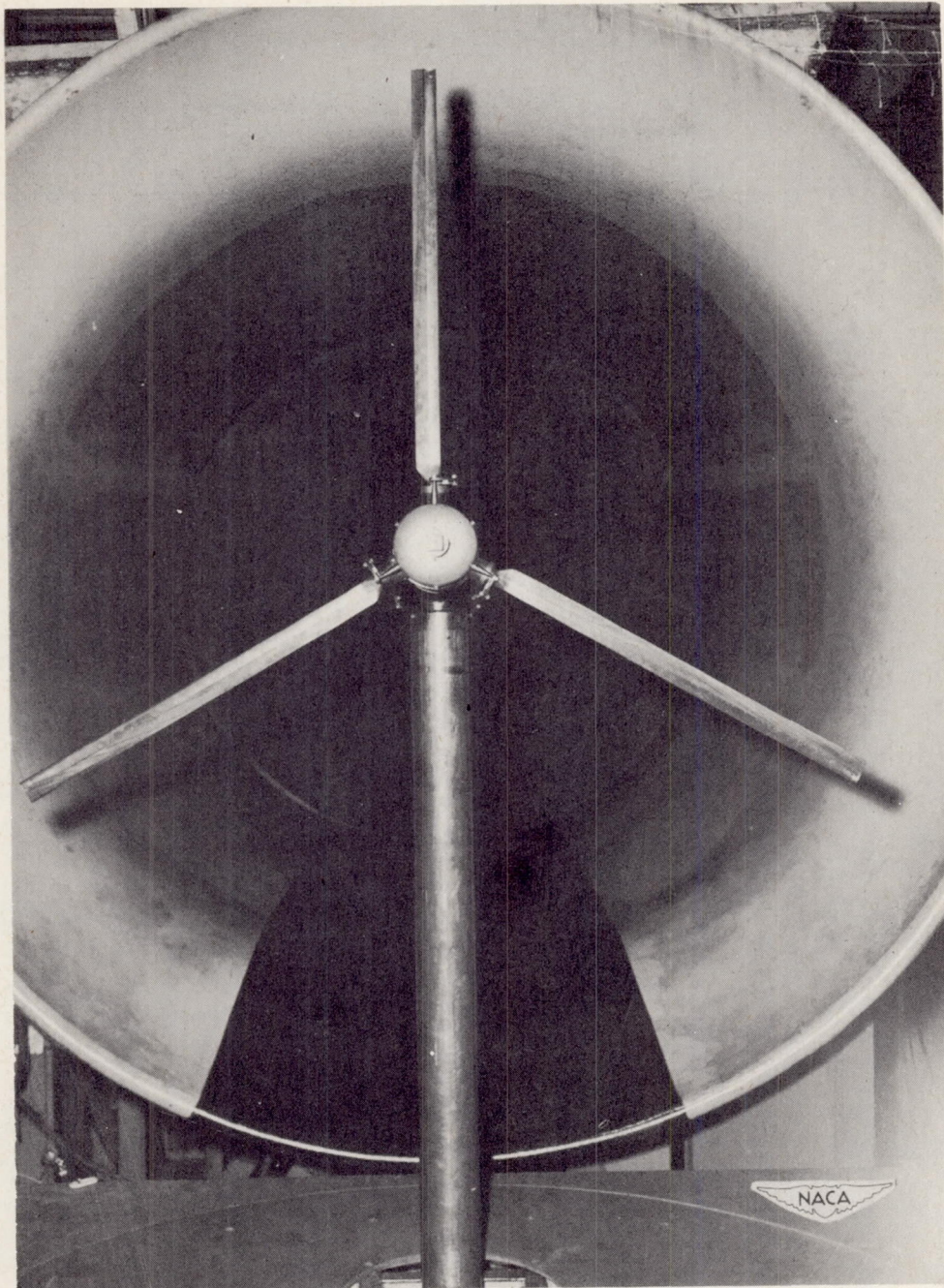
Figure 1.- Test stand with 6-foot-diameter rotor installed (apparent diameter of rotor exaggerated by perspective).
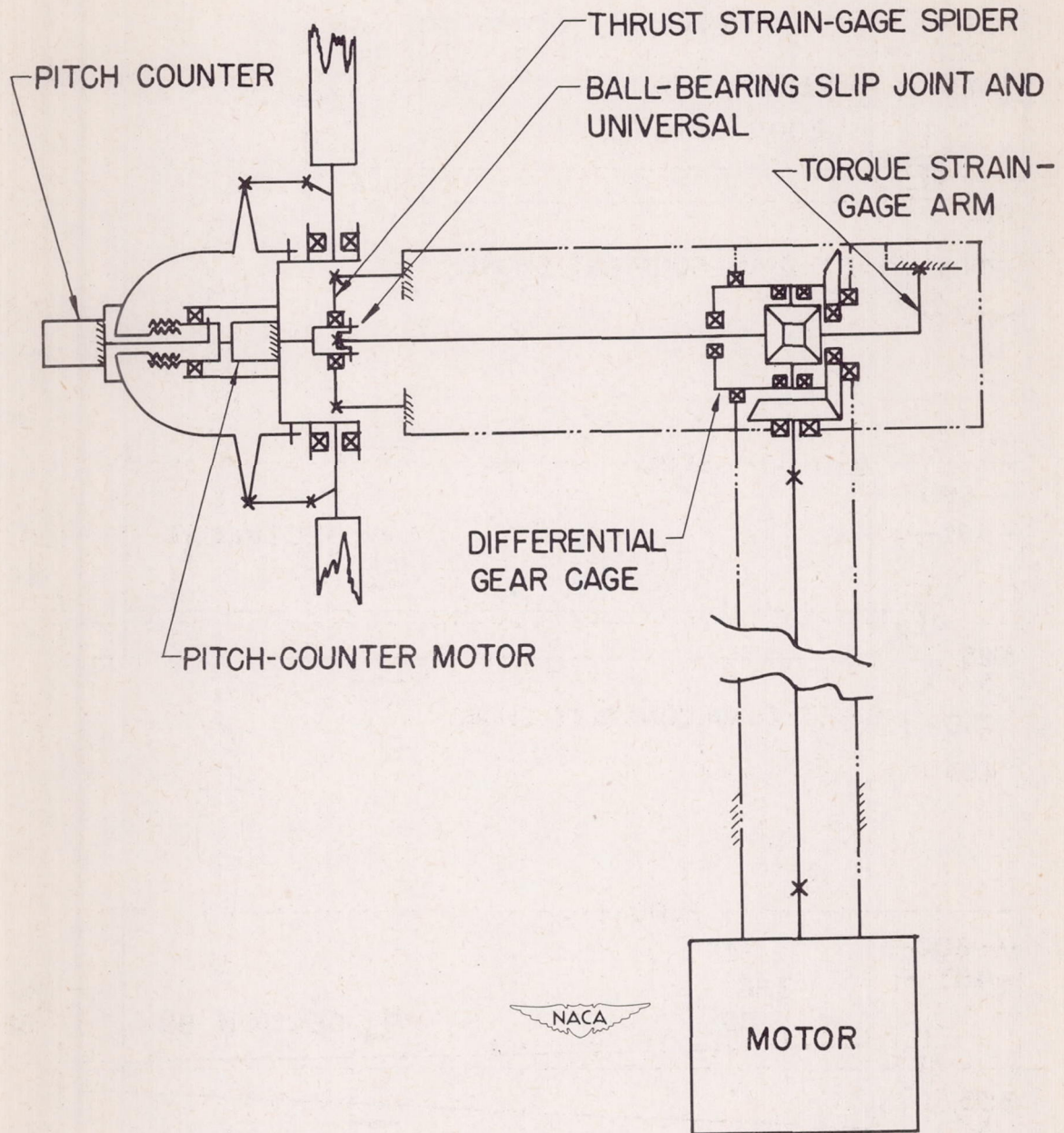
Figure 2.- Schematic drawing of test stand.
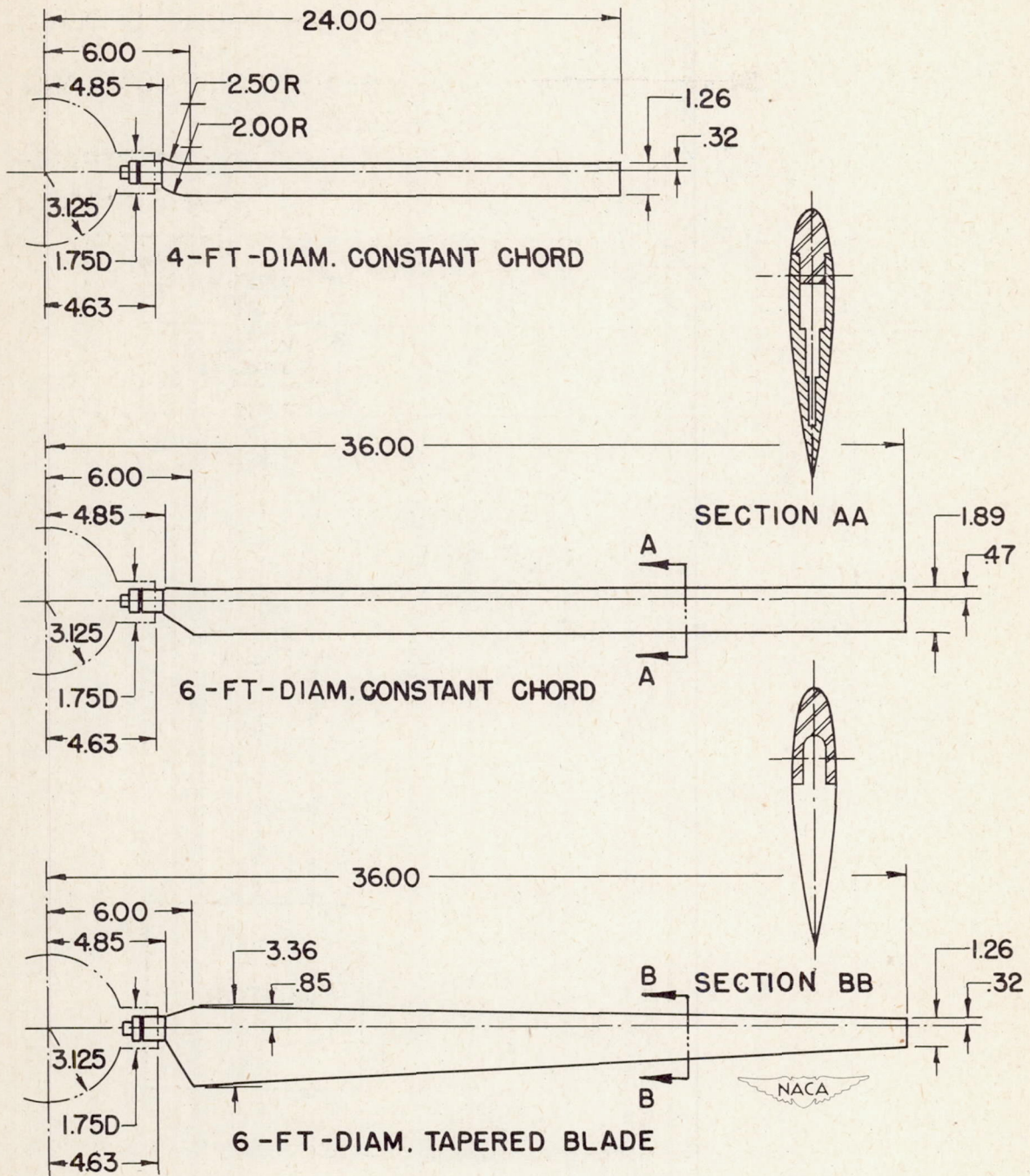
Figure 3.- Principal blade dimensions.
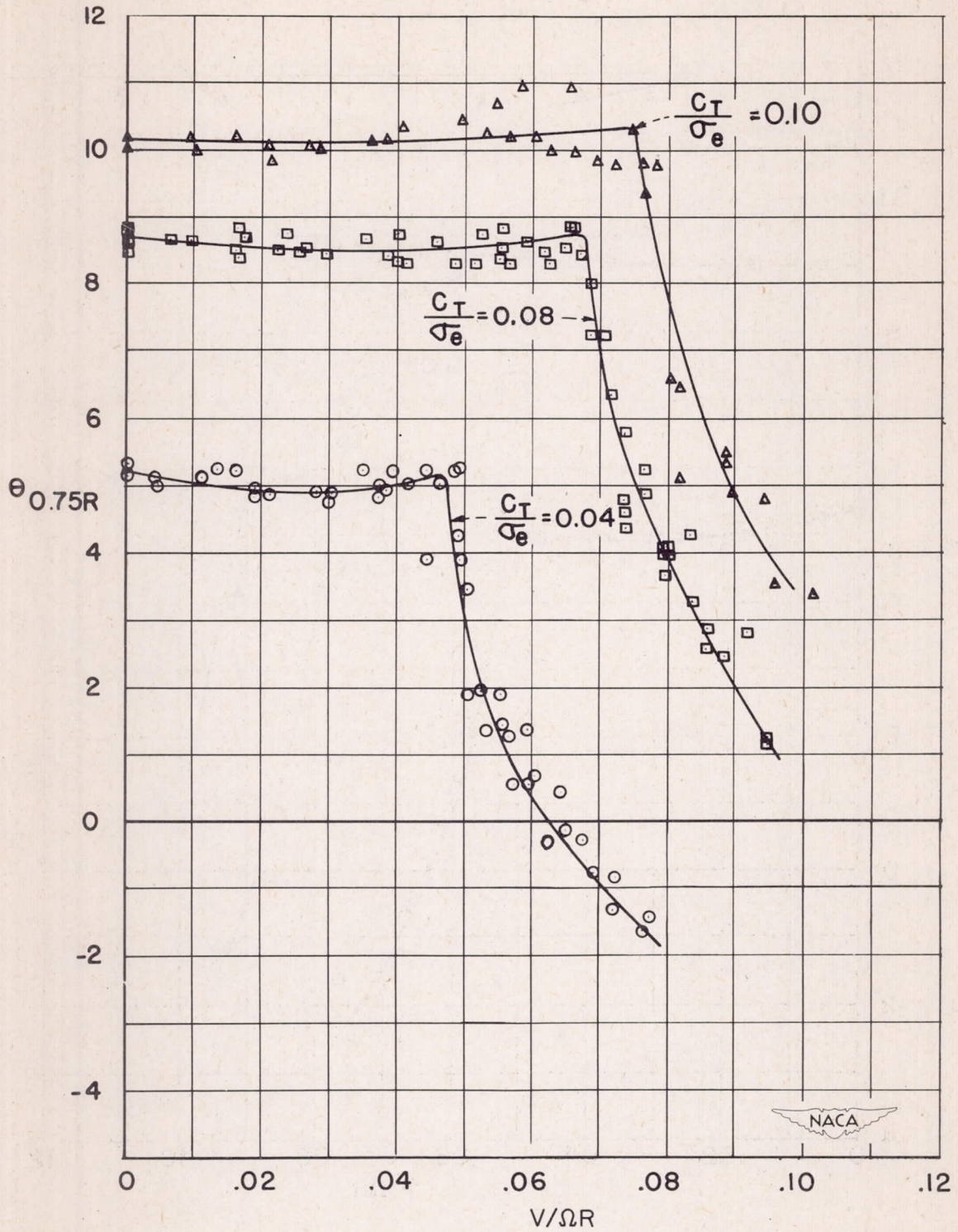
Figure 4.- Blade angles for 6-foot-diameter rotor with constant-chord, untwisted blades.
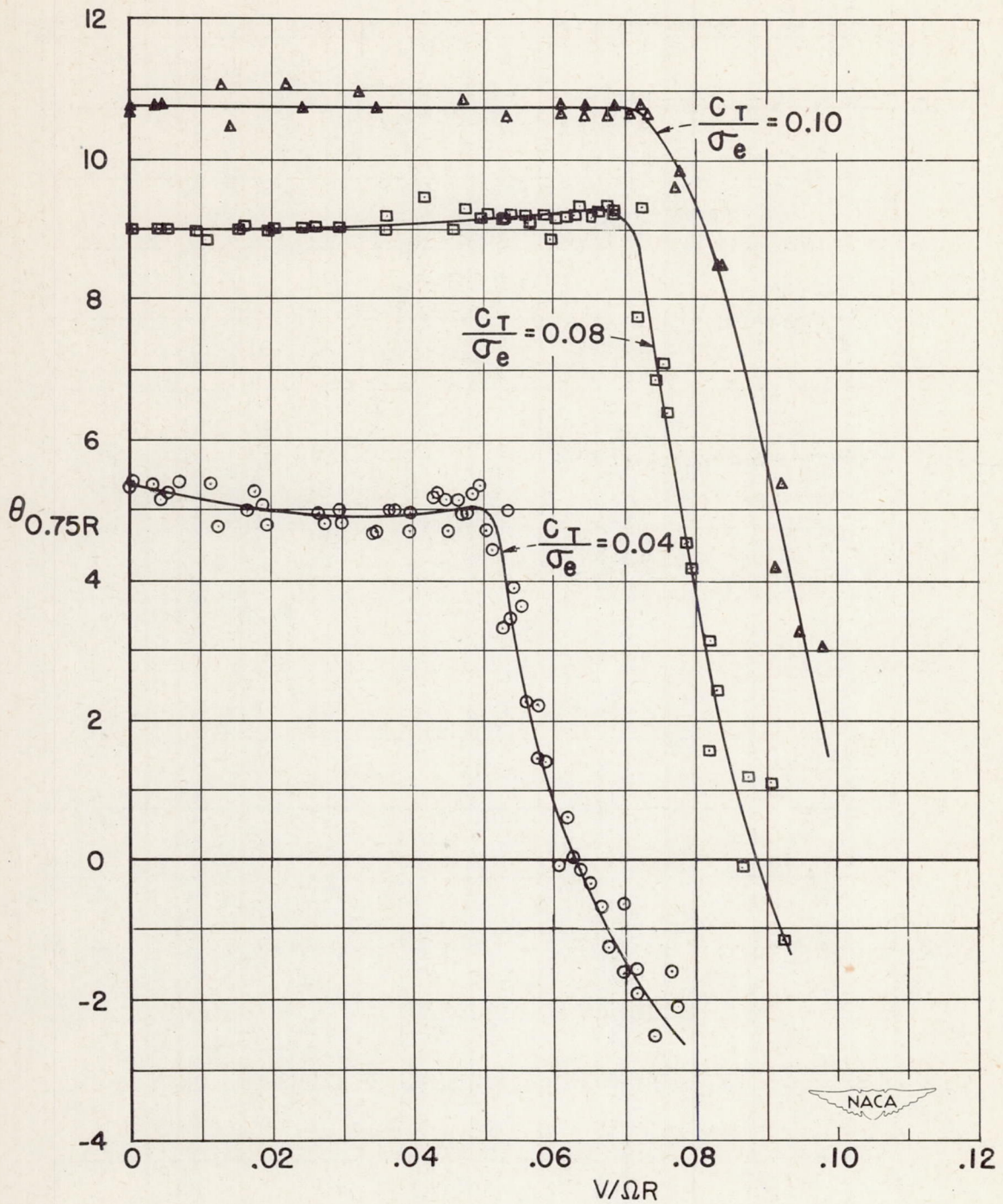
Figure 5.- Blade angles for 6-foot-diameter rotor with 3/1 tapered blades.
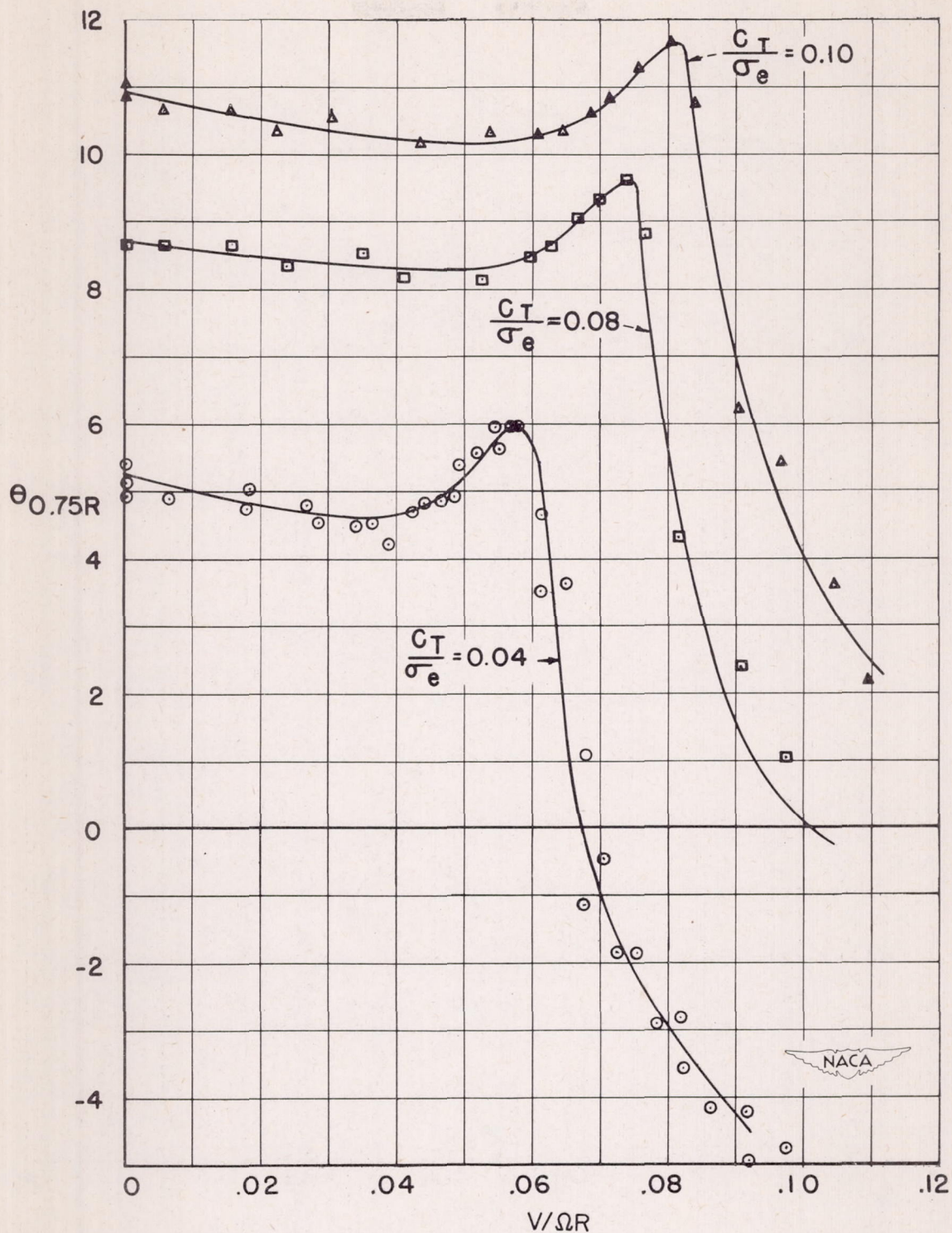
Figure 6.- Blade angles for 6-foot-diameter rotor with blades having 12° linear twist.
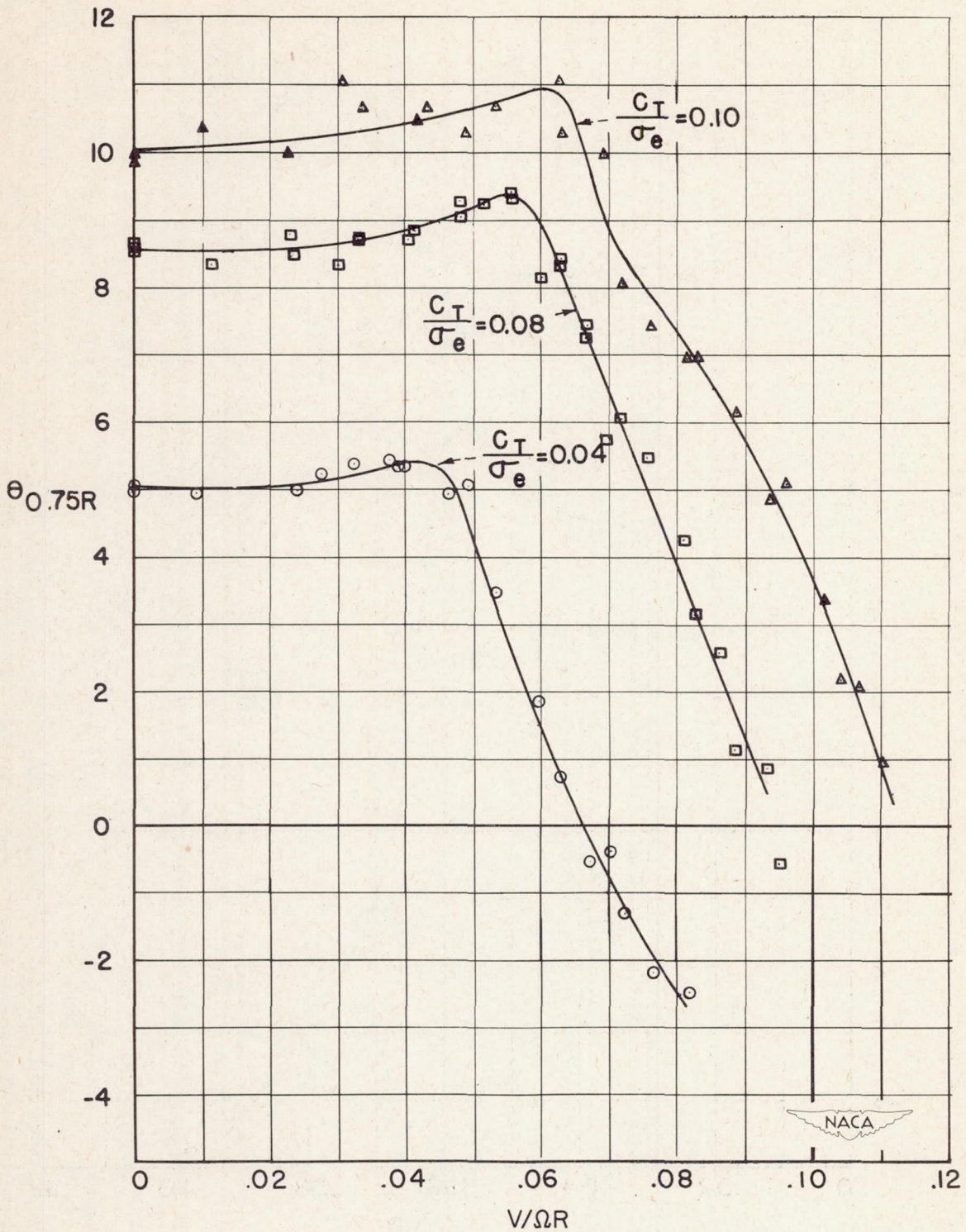
Figure 7.- Blade angles for 4-foot-diameter rotor with constant-chord, untwisted blades.
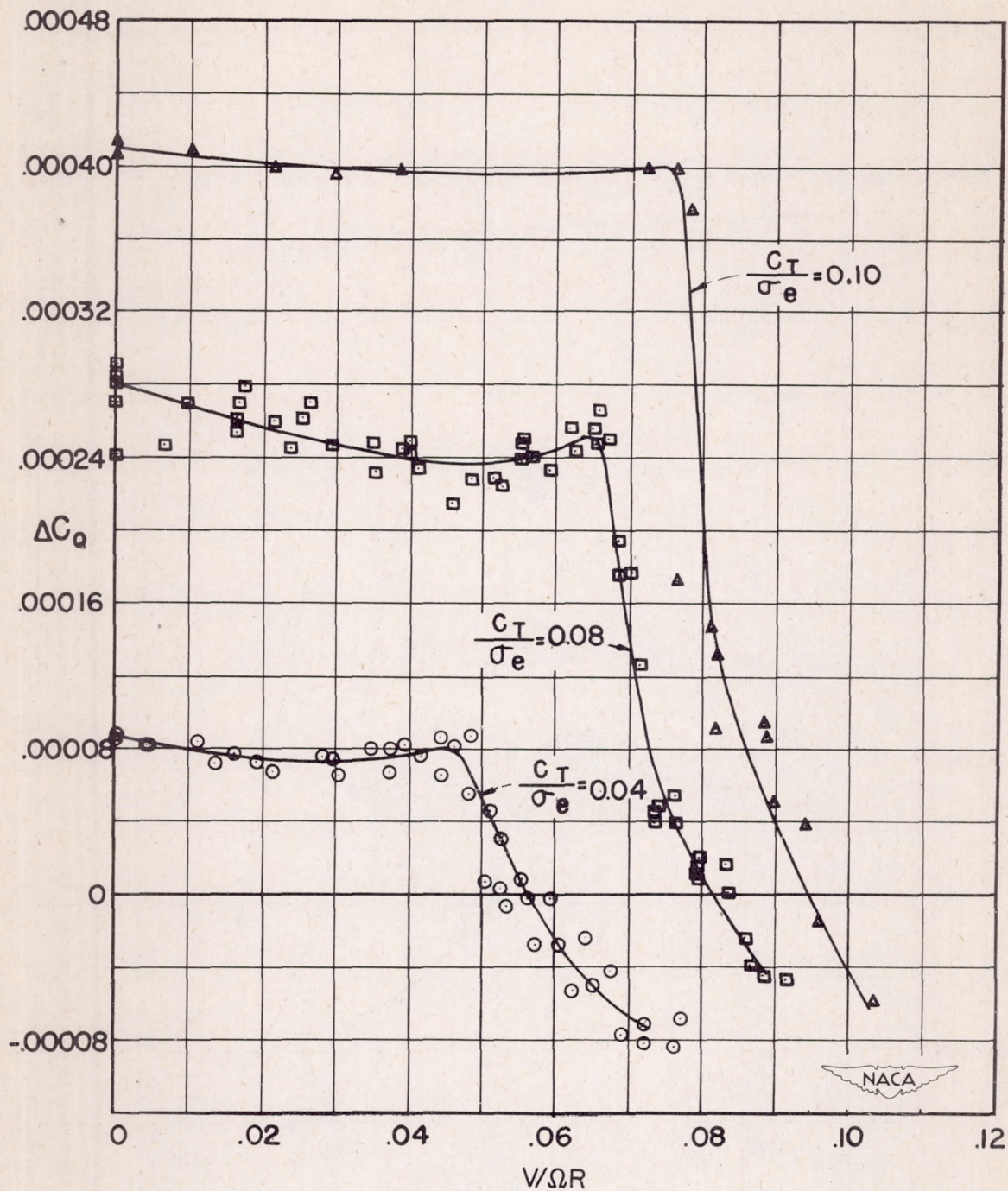
Figure 8.- Variation of torque coefficient for 6-foot-diameter rotor with constant-chord, untwisted blades.
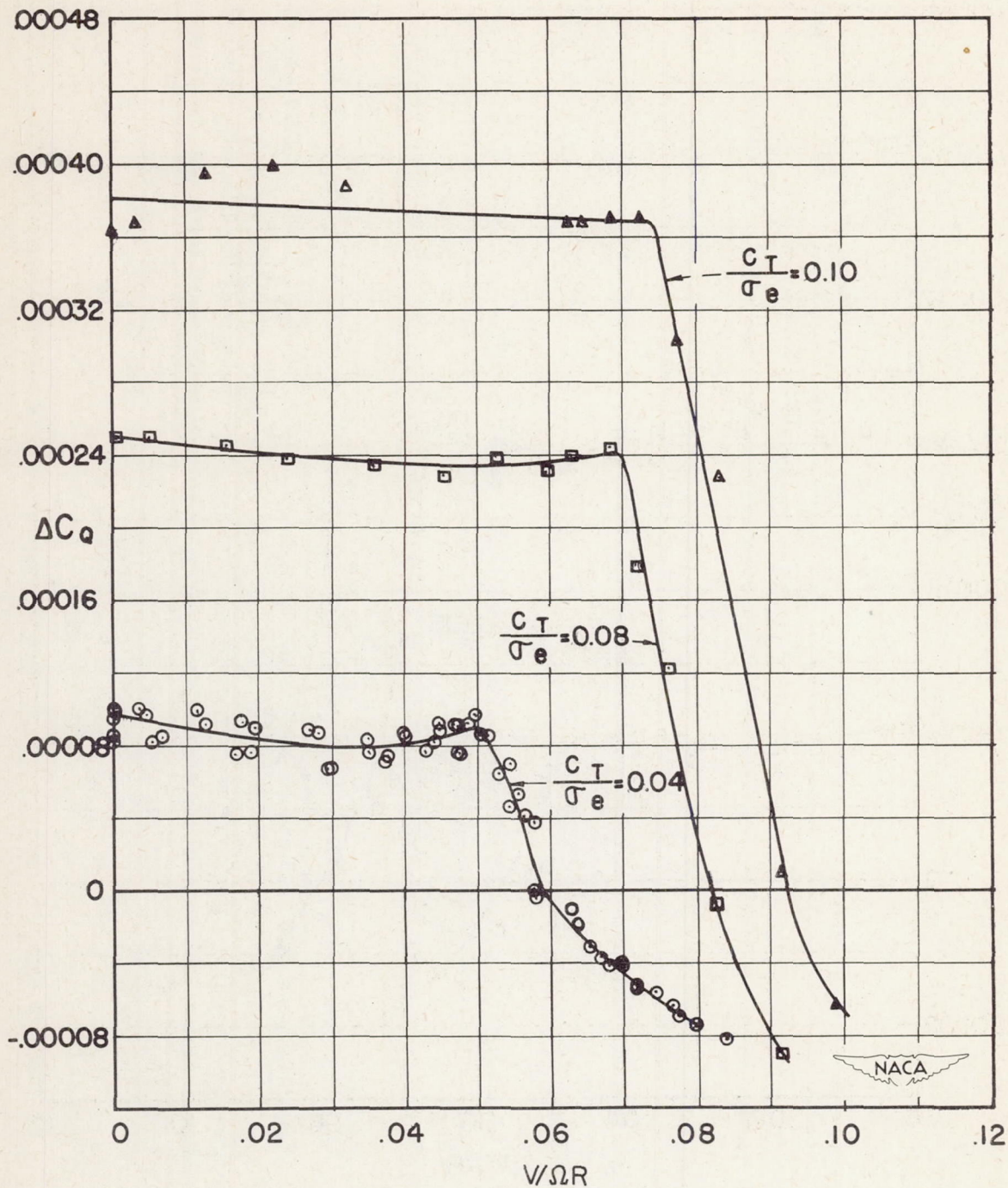
Figure 9.- Variation of torque coefficient for 6-foot-diameter rotor with 3/1 tapered blades.
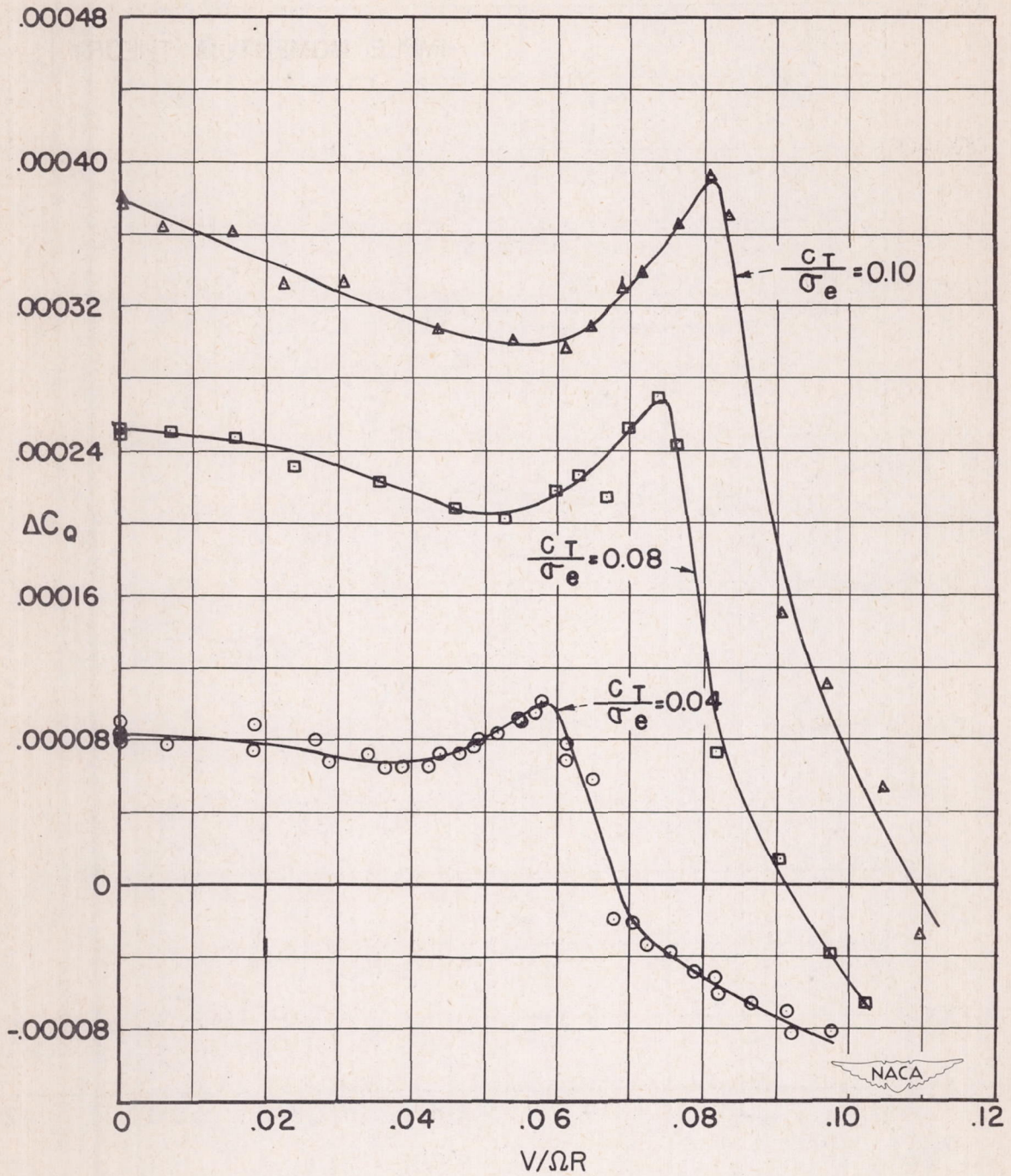
Figure 10.- Variation of torque coefficient for 6-foot-diameter rotor with blades having 12° linear twist.
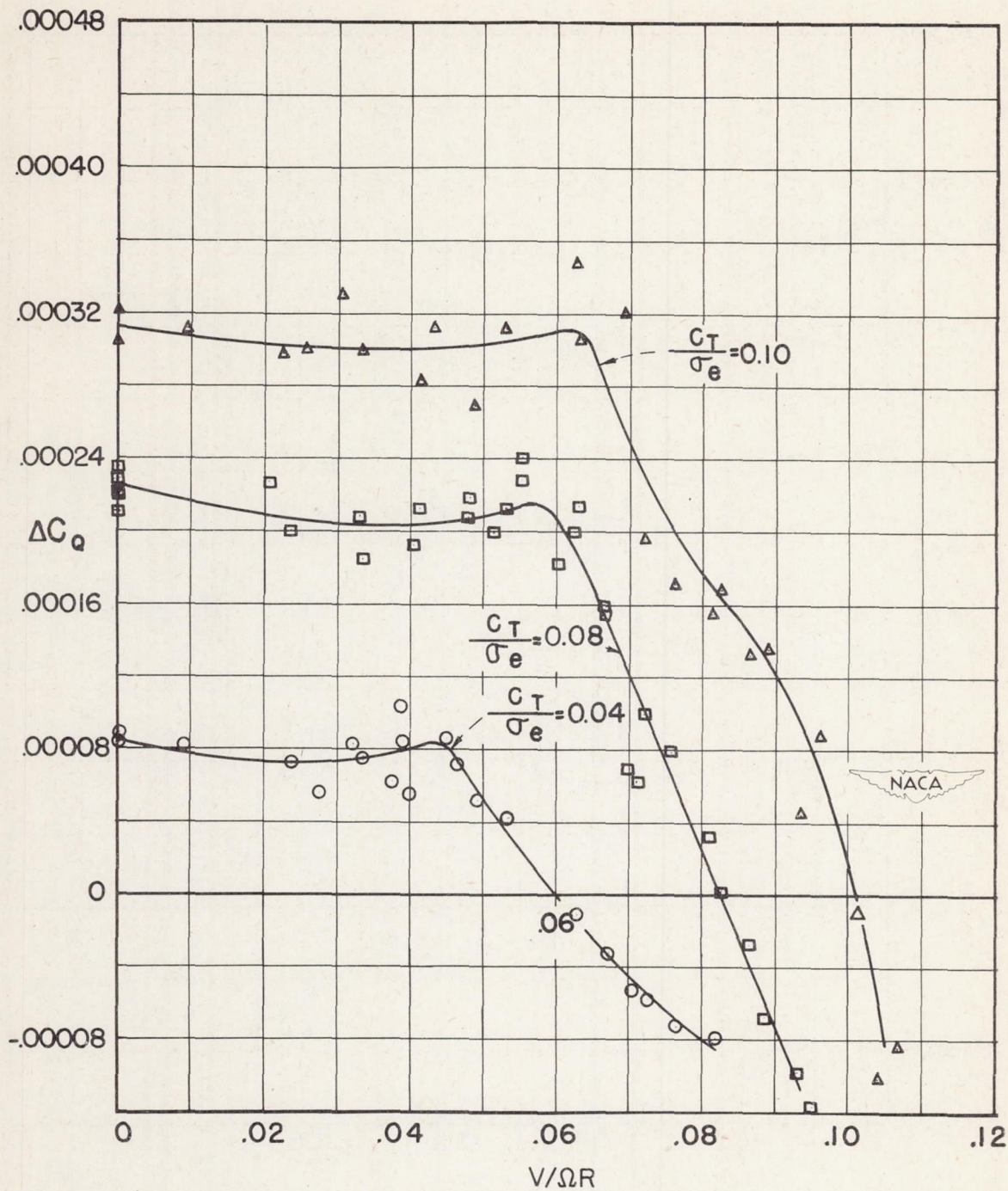
Figure 11.- Variation of torque coefficient for 4-foot-diameter rotor
with constant-chord, untwisted blades.
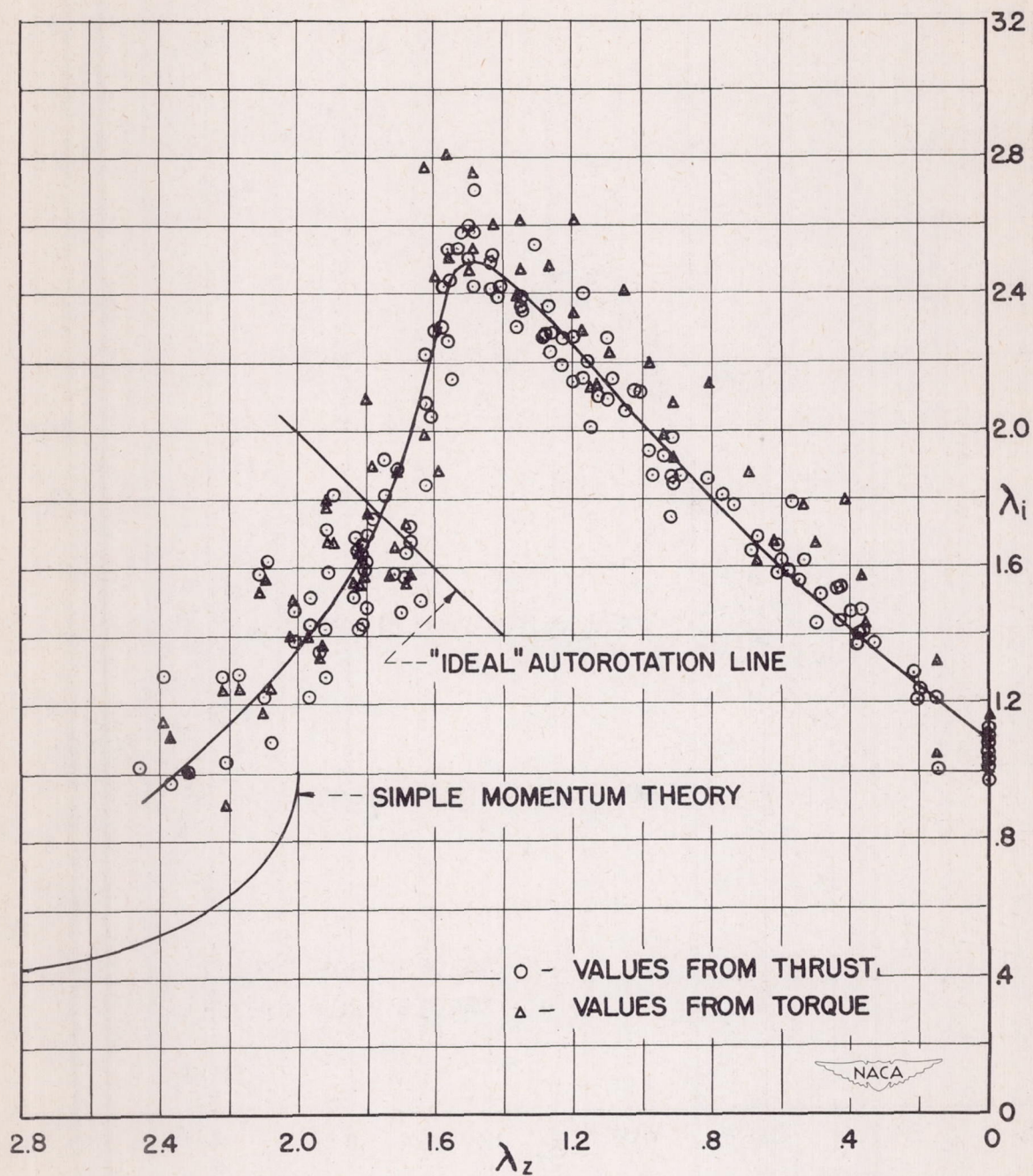
Figure 12.- Variation of nondimensional induced velocity for 6-foot-
diameter rotor with constant-chord, untwisted blades.
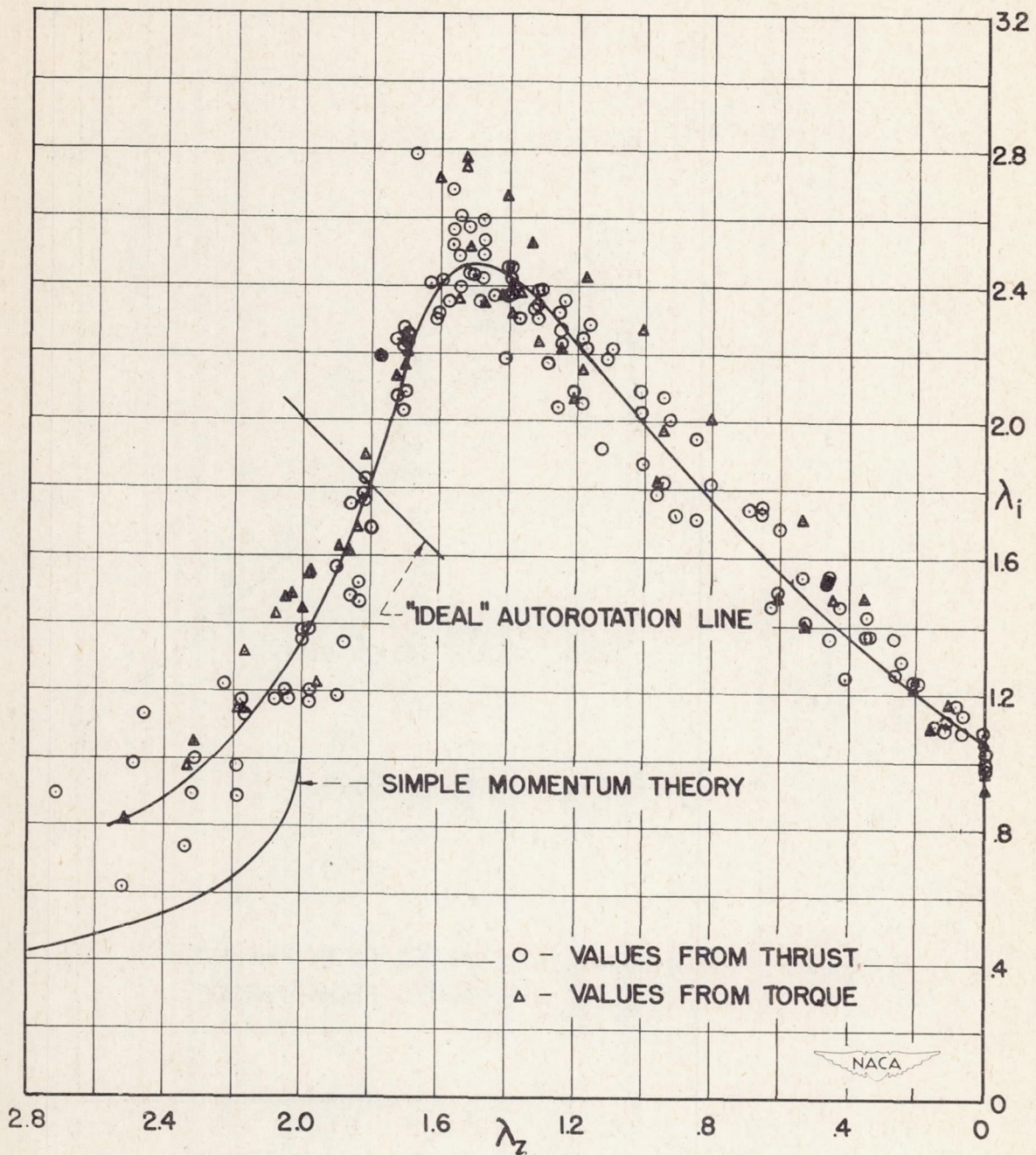
Figure 13.– Variation of nondimensional induced velocity for 6-foot-
diameter rotor with 3/1 tapered blades.
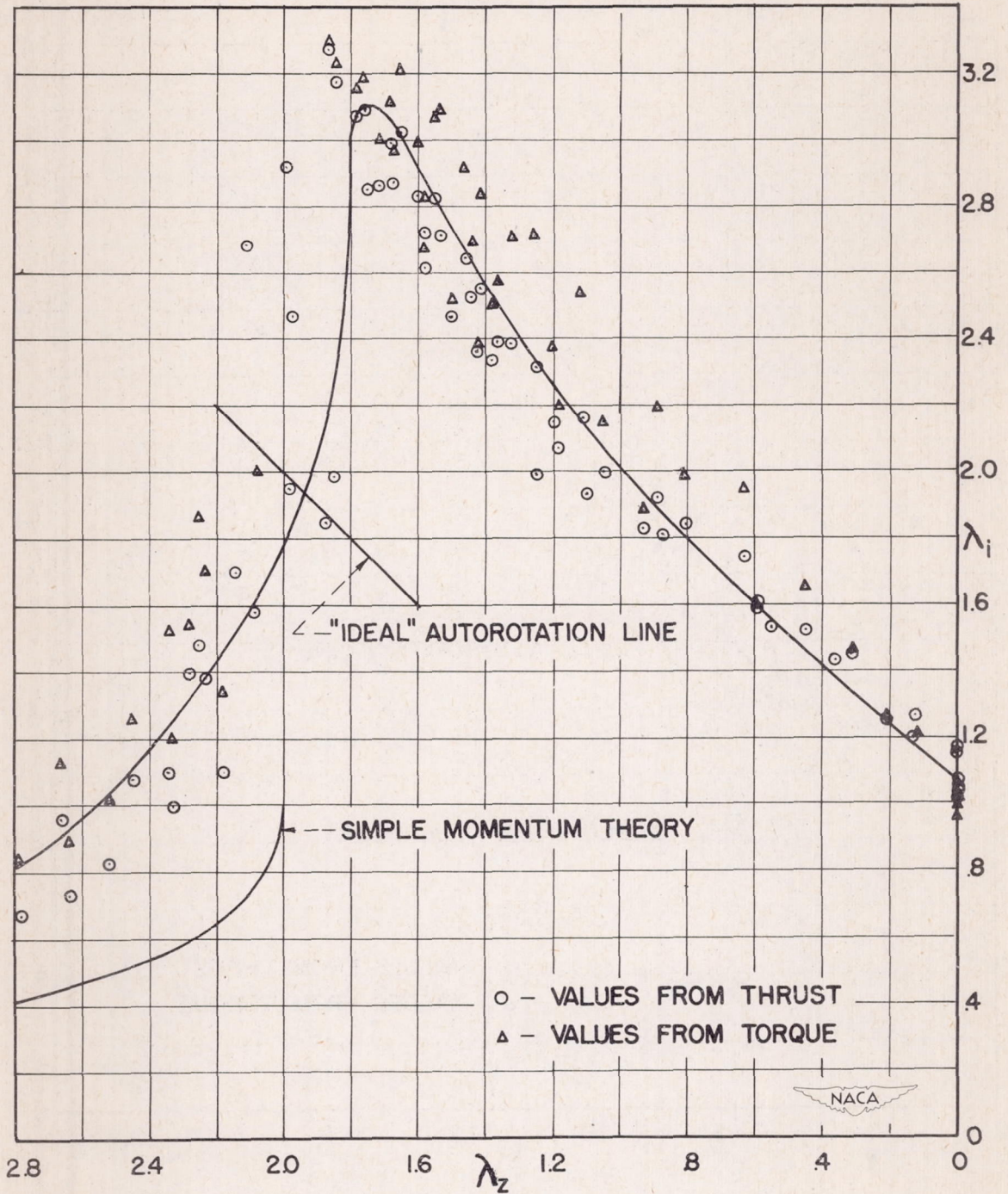
Figure 14.- Variation of nondimensional induced velocity for 6-foot-diameter rotor with blades having 12° linear twist.
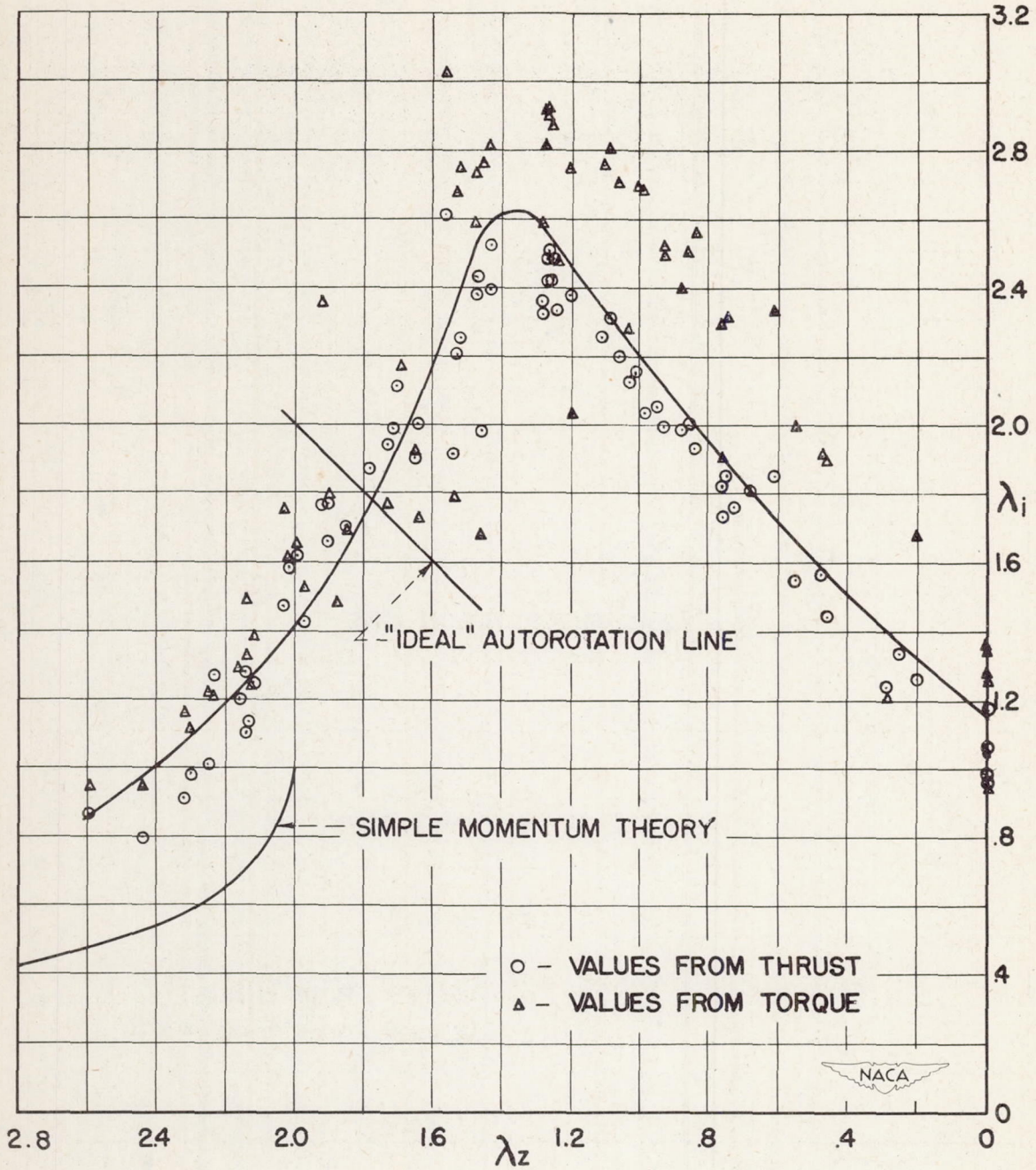
Figure 15.- Variation of nondimensional induced velocity for 4-foot-
diameter rotor with constant-chord, untwisted blades.
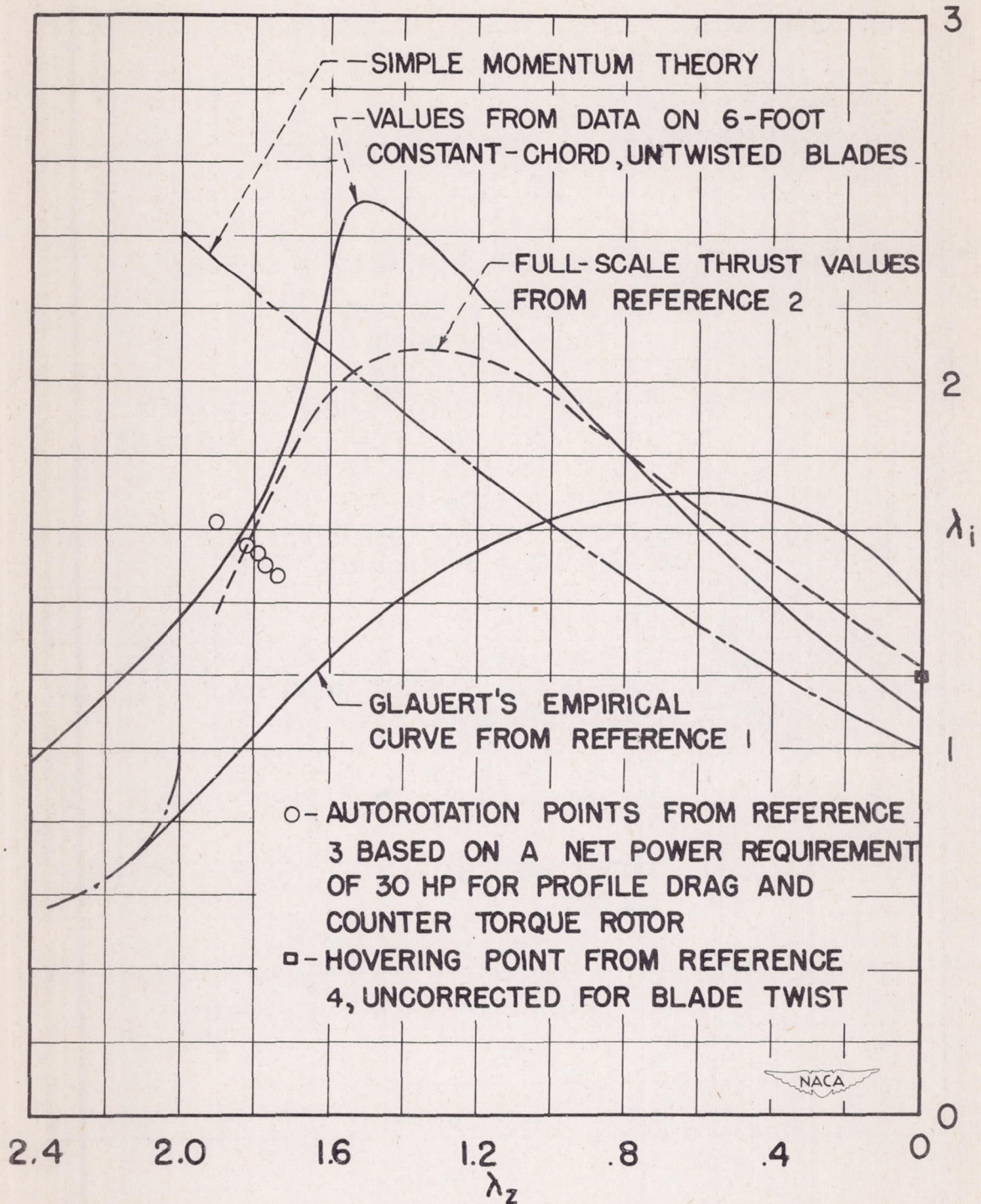
Figure 16.- Comparison of data on λ_i against λ_z coordinates.
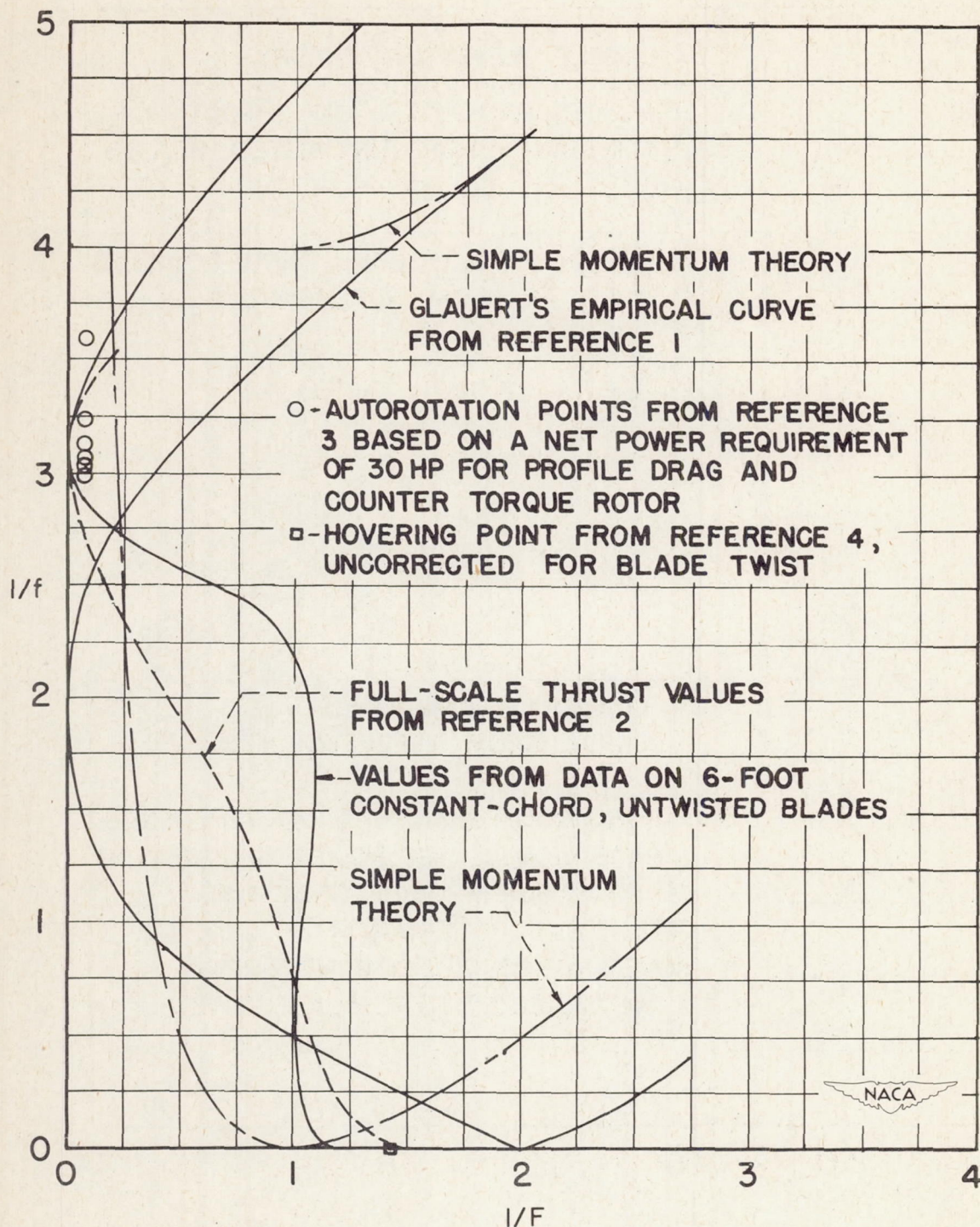
Figure 17.- Comparison of data on 1/f against 1/F coordinates.
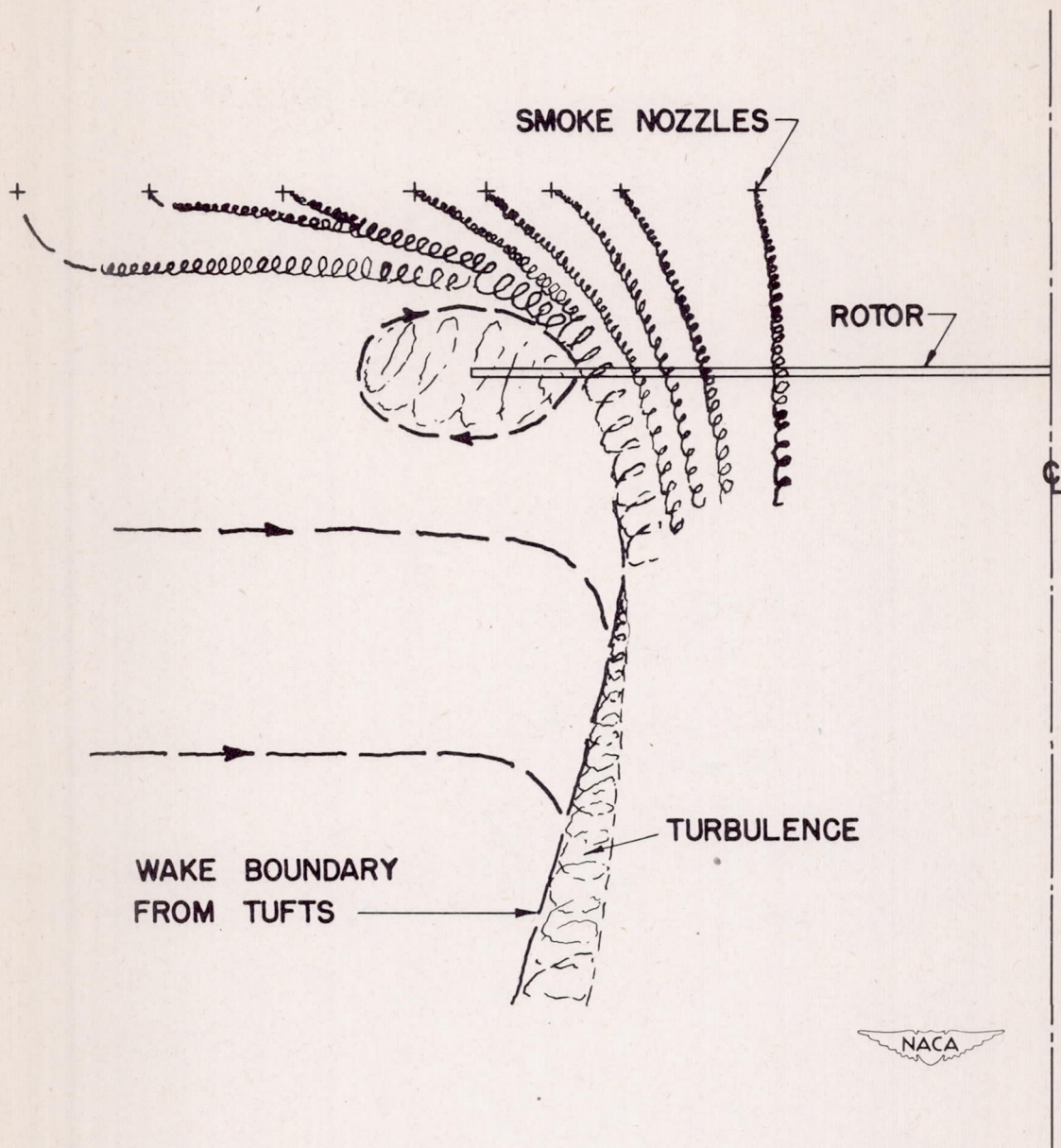
Figure 18.- Flow pattern at $\lambda_z = 0$ (hovering) for 4-foot-diameter rotor with constant-chord, untwisted blades.
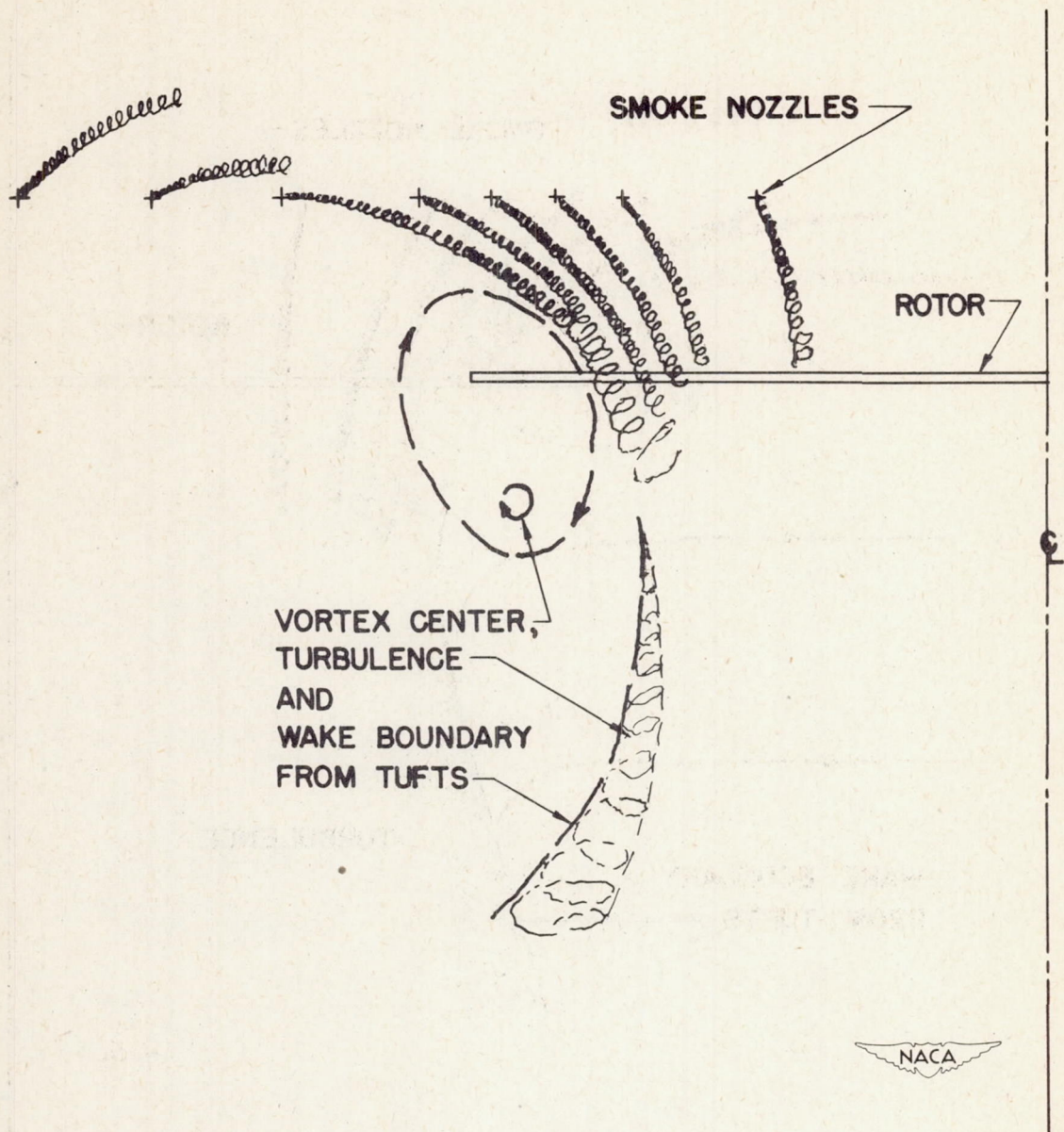
Figure 19.- Flow pattern at $\lambda_z \approx 0.3$ for 4-foot-diameter rotor with constant-chord, untwisted blades.
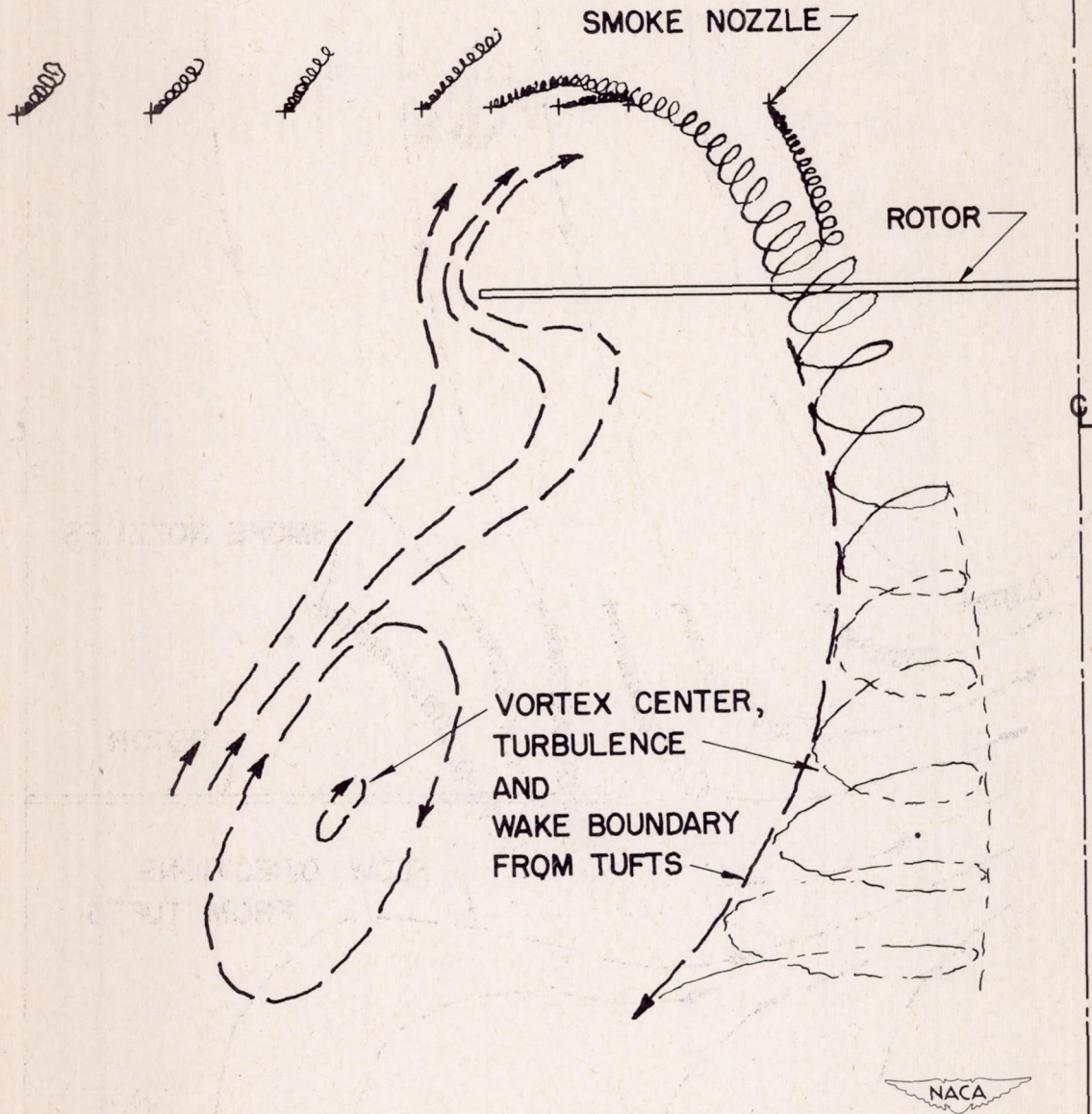
Figure 20.- Flow pattern at $\lambda_z \approx 1.0$ for 4-foot-diameter rotor with constant-chord, untwisted blades.
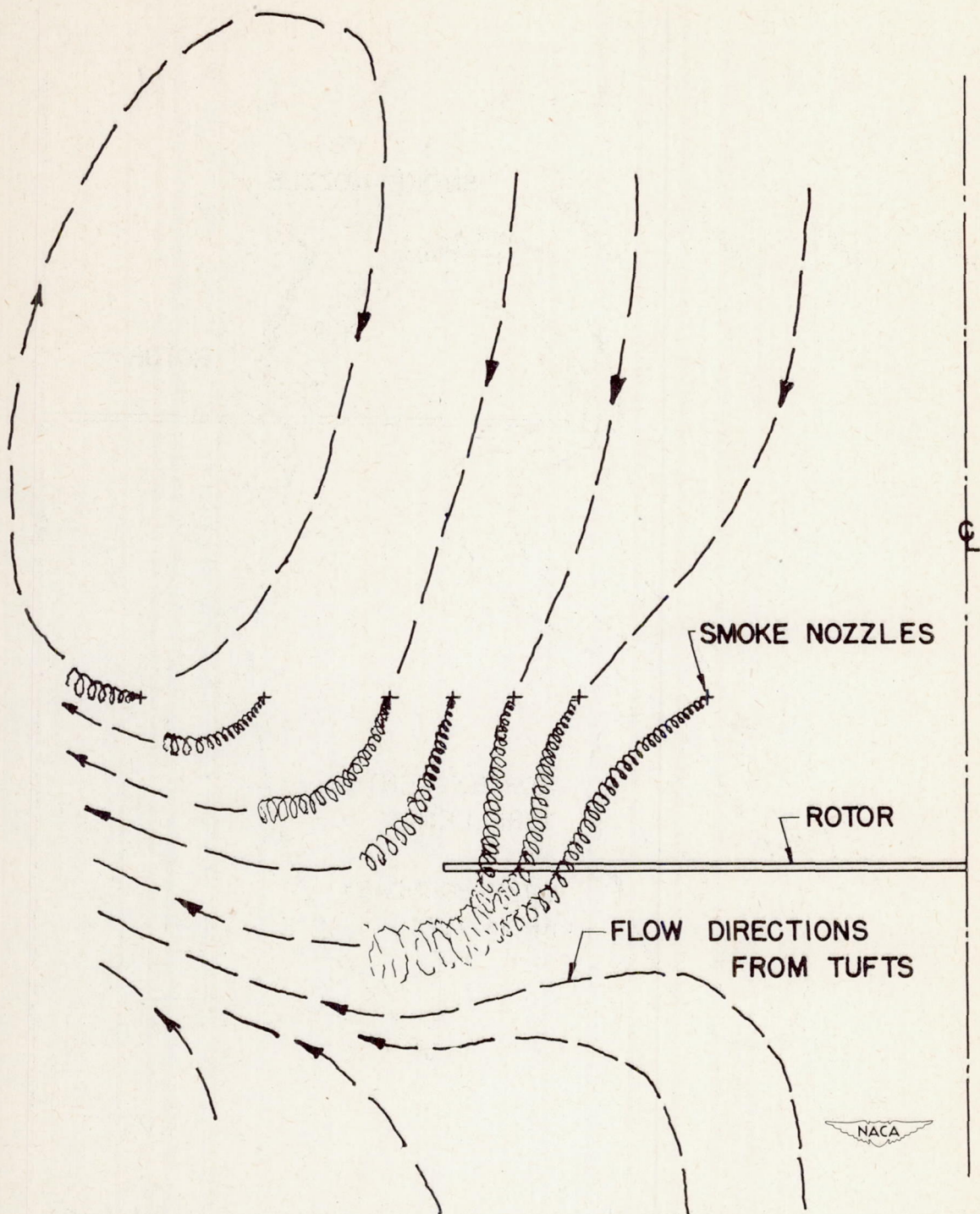
Figure 21.- Flow pattern at $\lambda_z \approx 1.35$ for 4-foot-diameter rotor with constant-chord, untwisted blades.
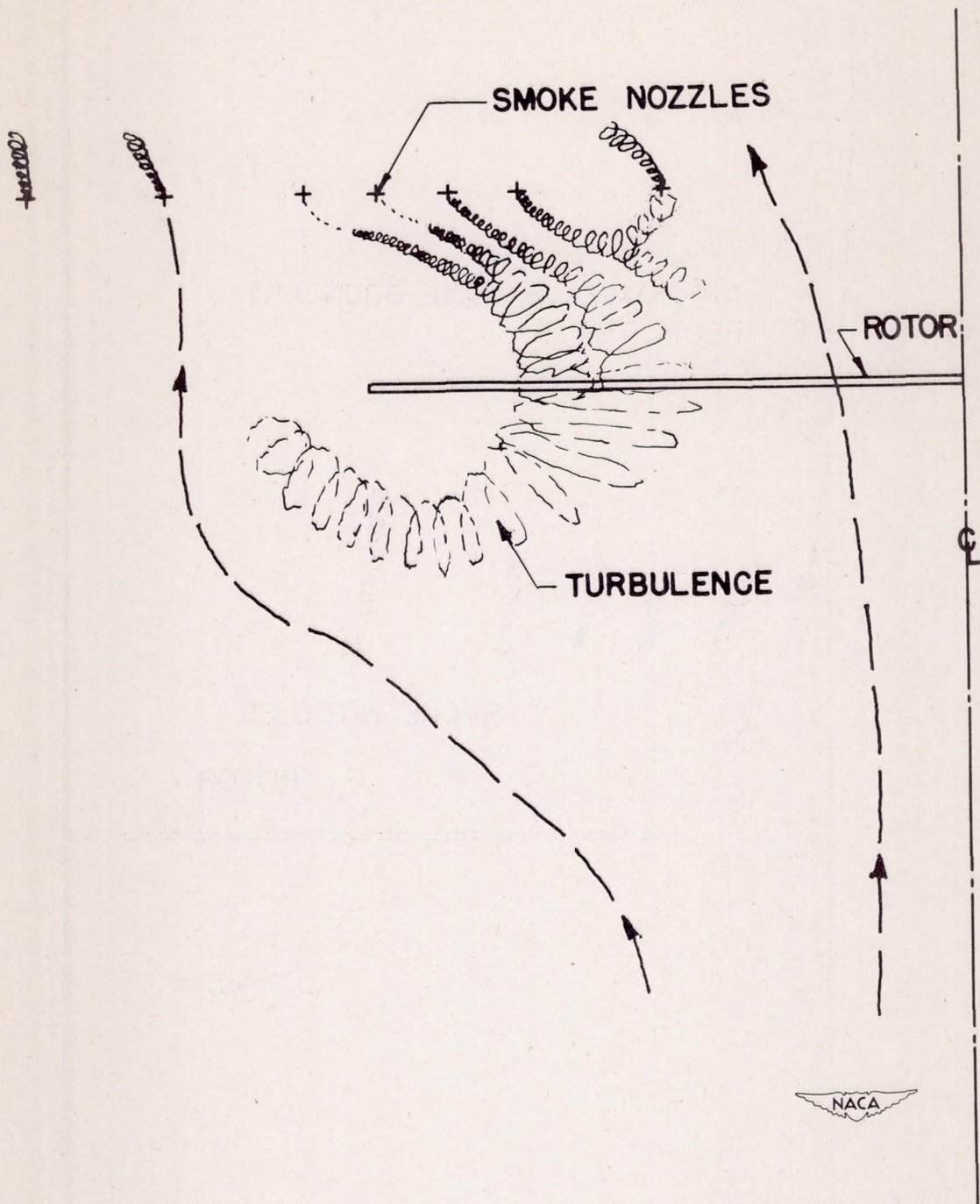
Figure 22.- Flow pattern at $\lambda_z \approx 1.7$ for 4-foot-diameter rotor with constant-chord, untwisted blades.
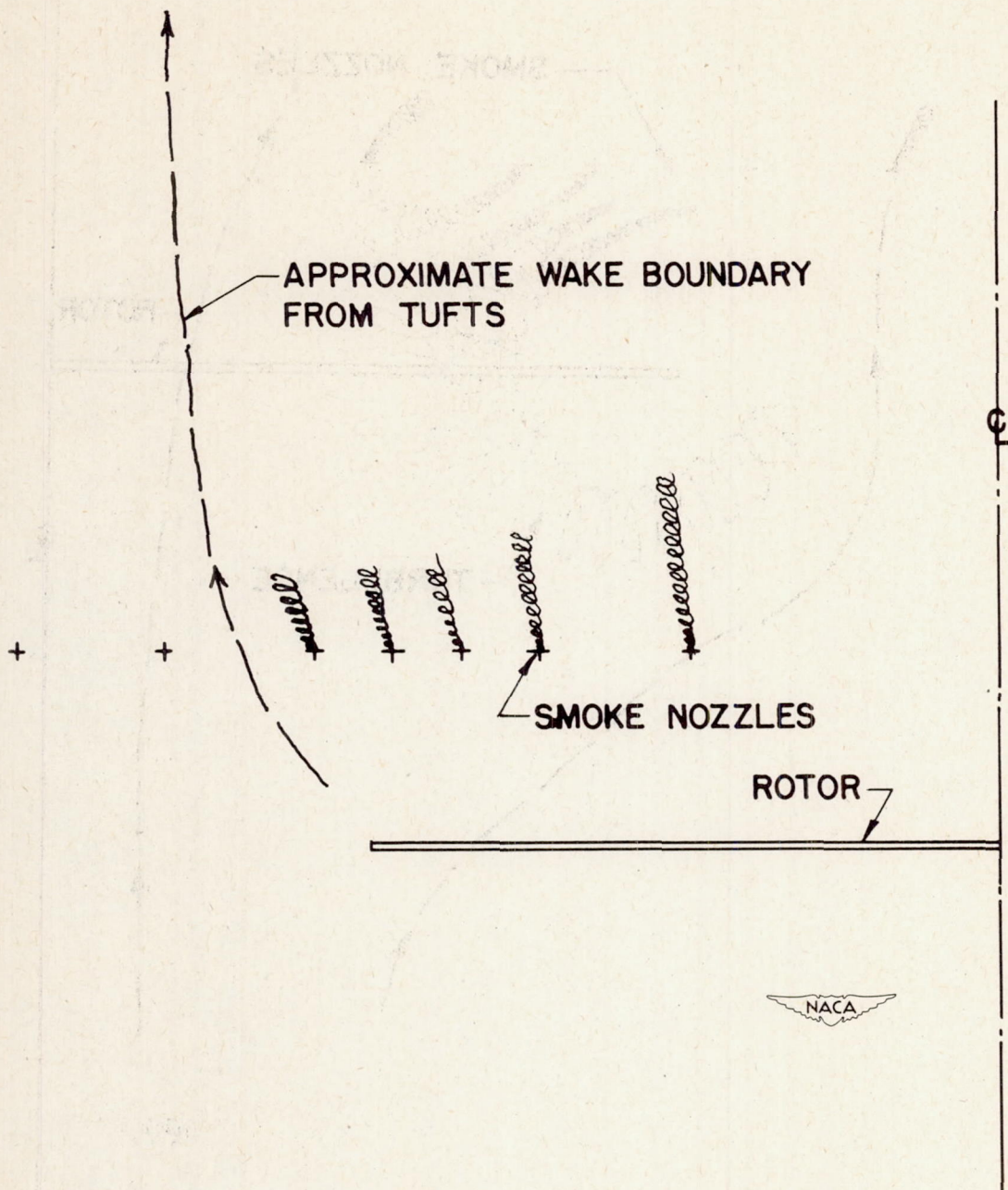
Figure 23.- Flow pattern at $\lambda_z \approx 2.0$ for 4-foot-diameter rotor with constant-chord, untwisted blades.
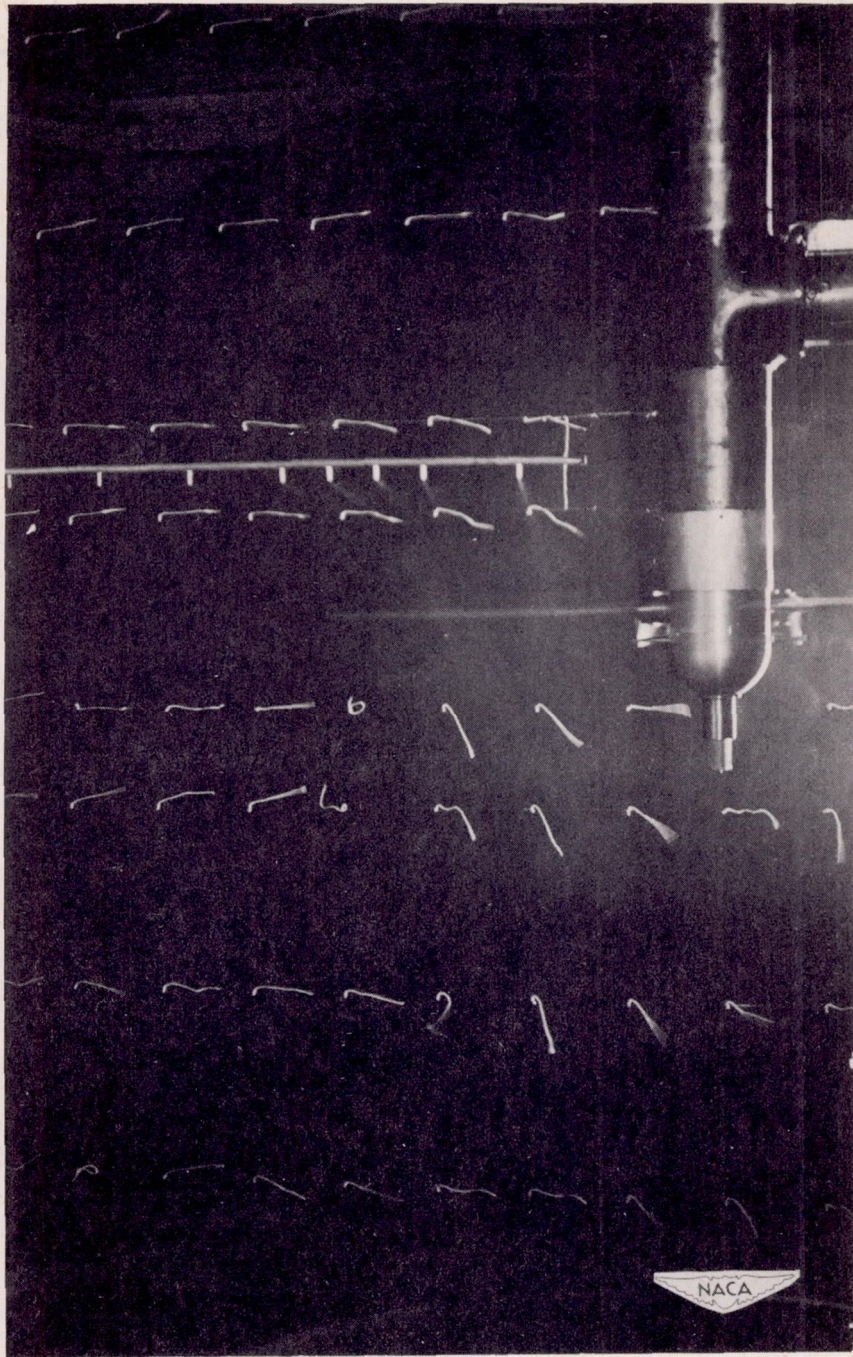
Figure 24.- Photograph of tufts and smoke filaments at $\lambda_z = 0.3$.
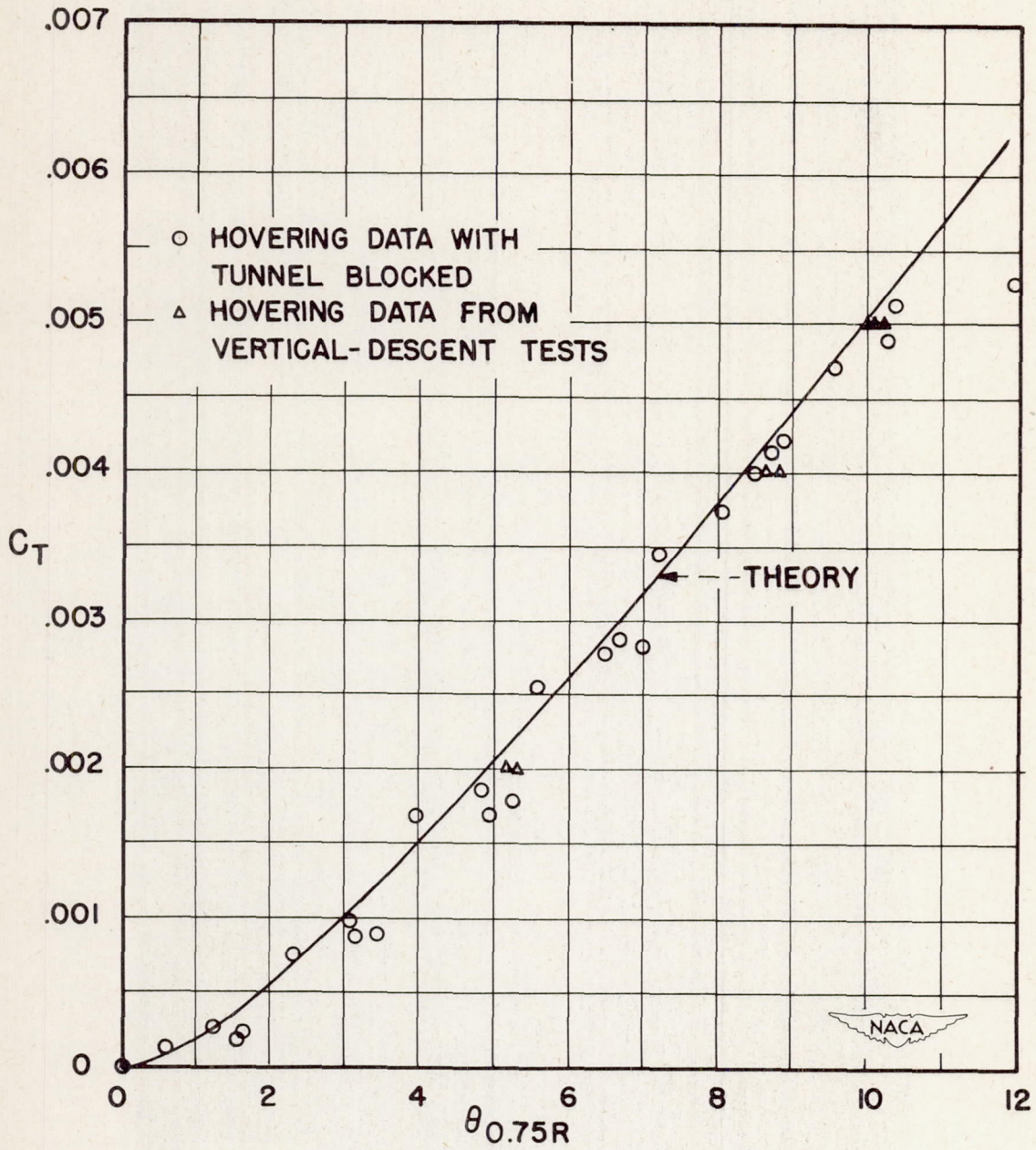
Figure 25.- Comparison of hovering data for 6-foot-diameter rotor with constant-chord, untwisted blades.
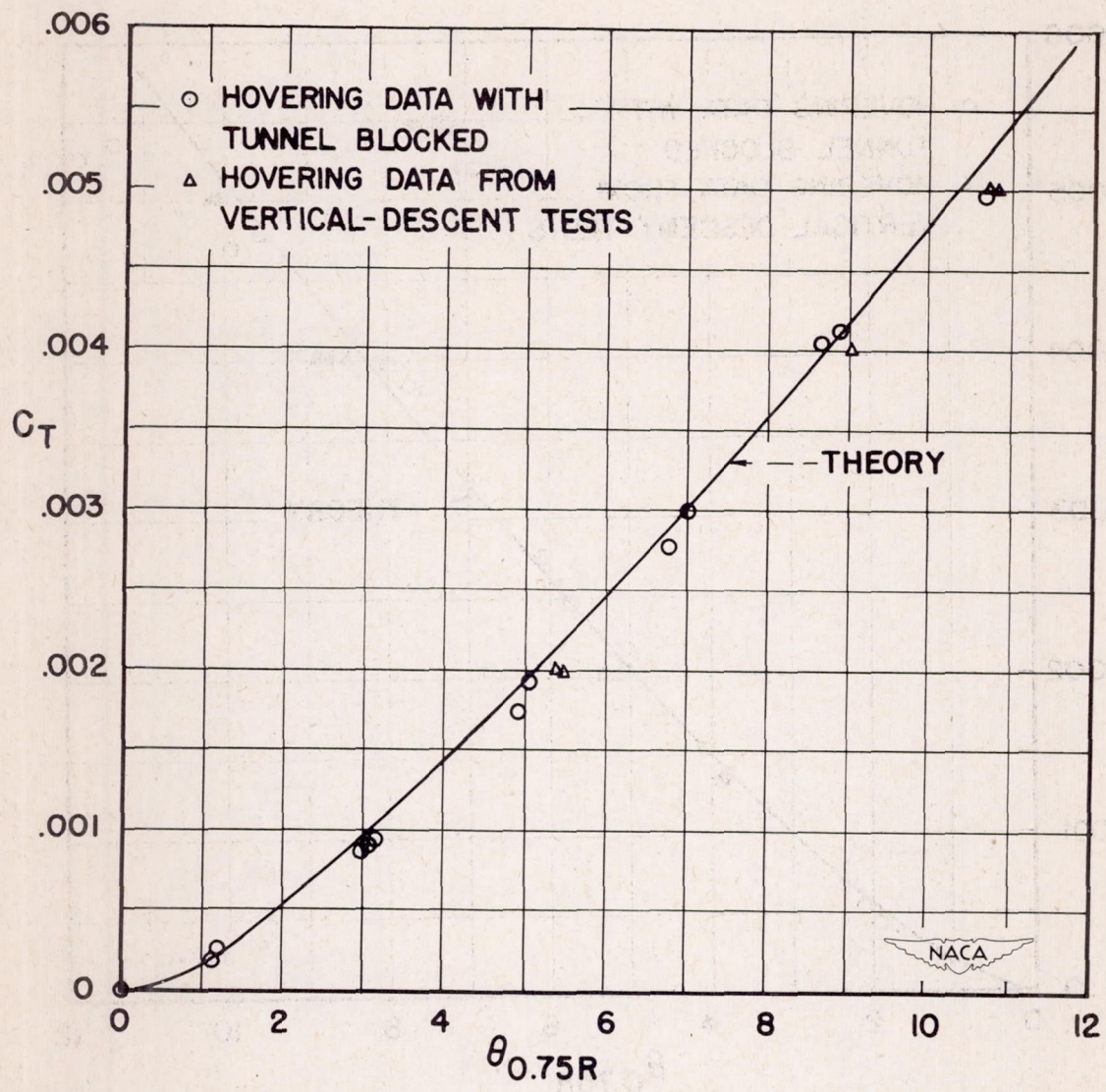
Figure 26.- Comparison of hovering data for 6-foot-diameter rotor with 3/1 tapered blades.
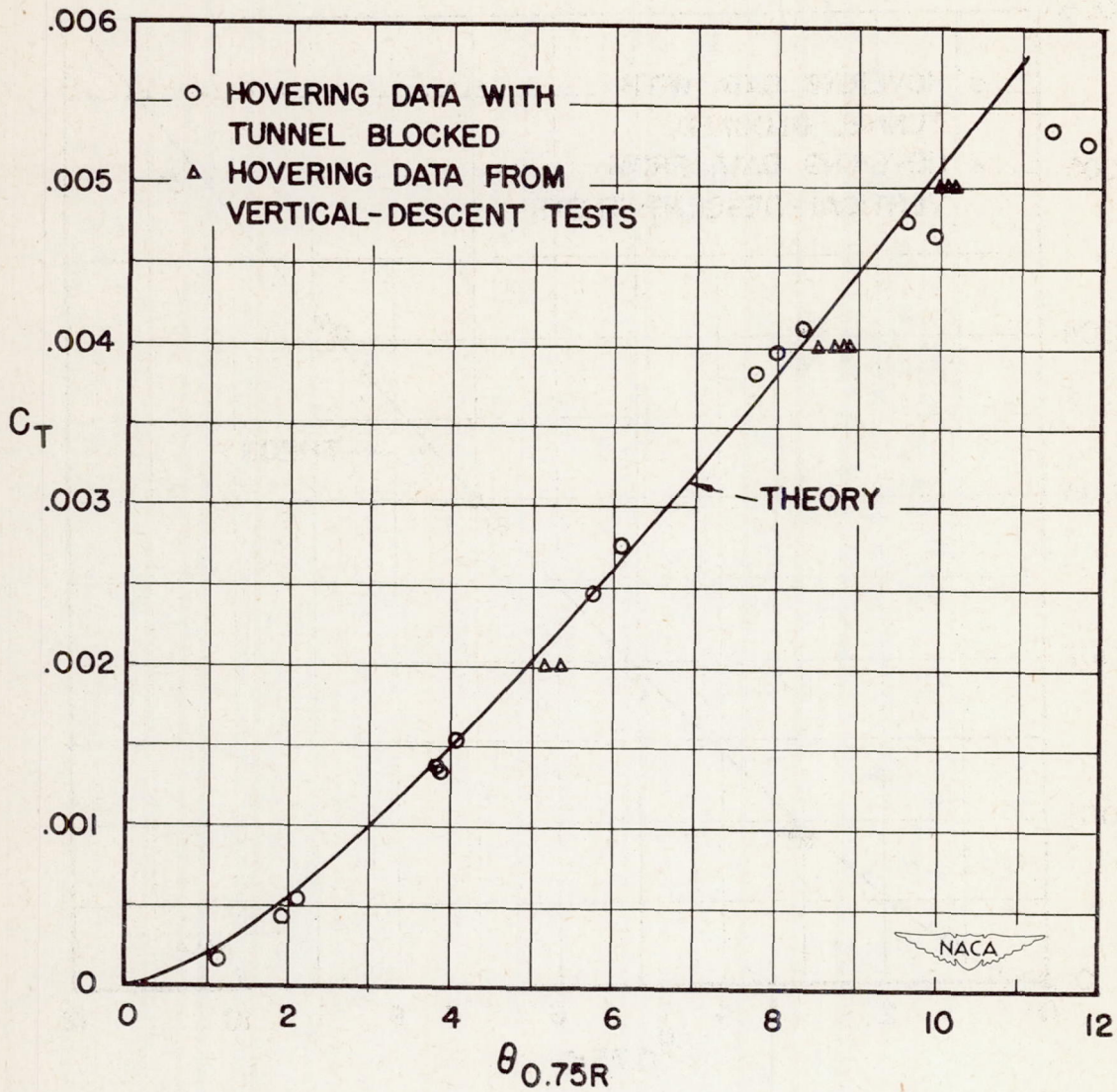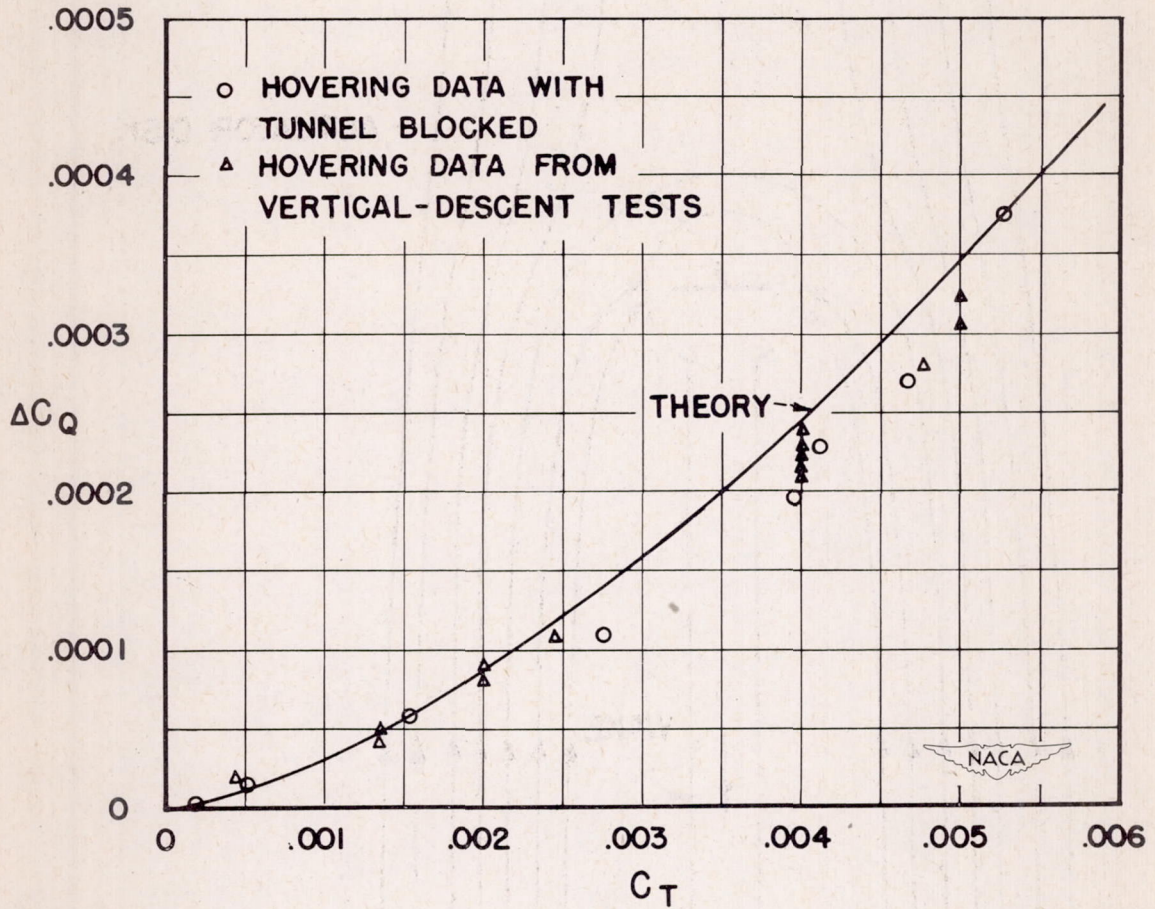
Figure 27.- Comparison of hovering data for 4-foot-diameter rotor with constant-chord, untwisted blades.
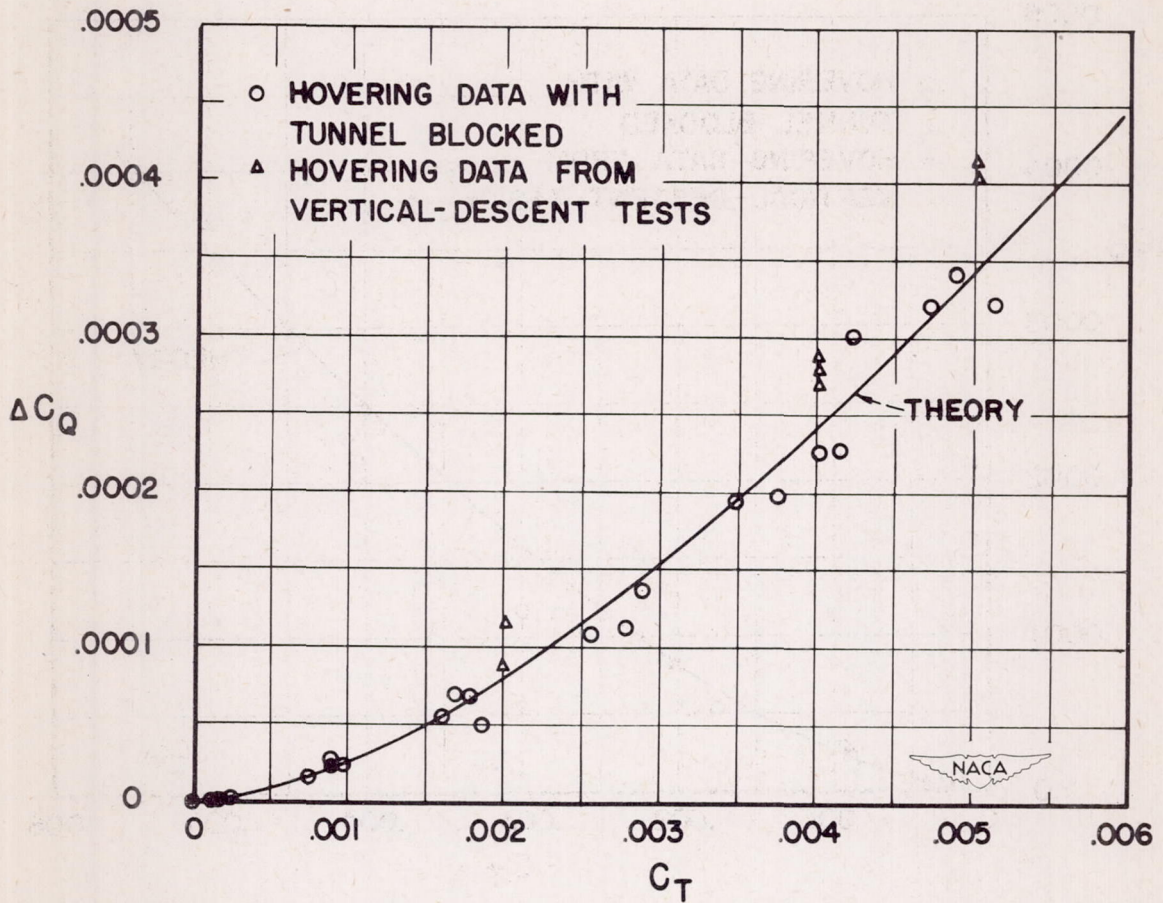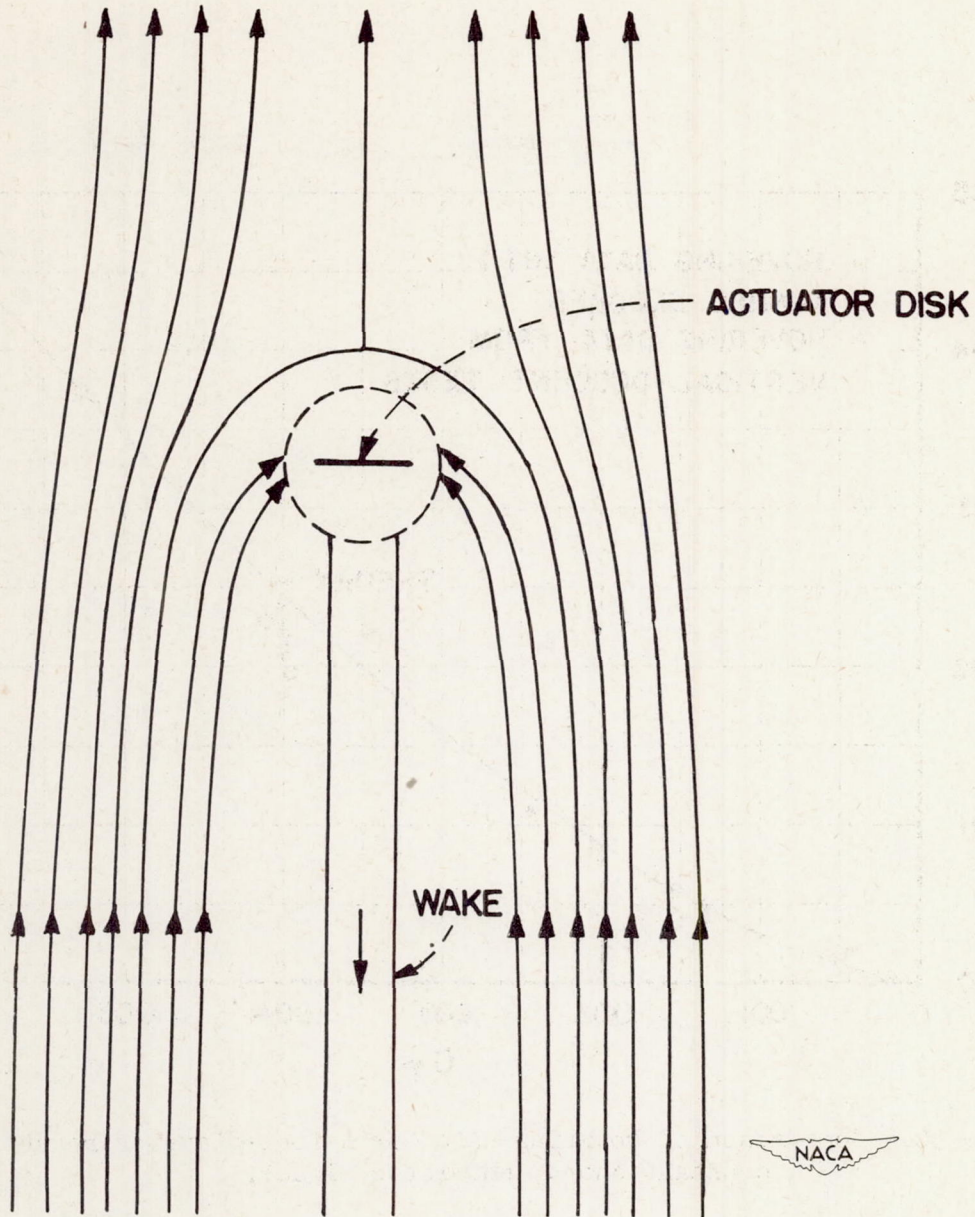
Figure 28.- Comparison of hovering data for 6-foot-diameter rotor with constant-chord, untwisted blades.
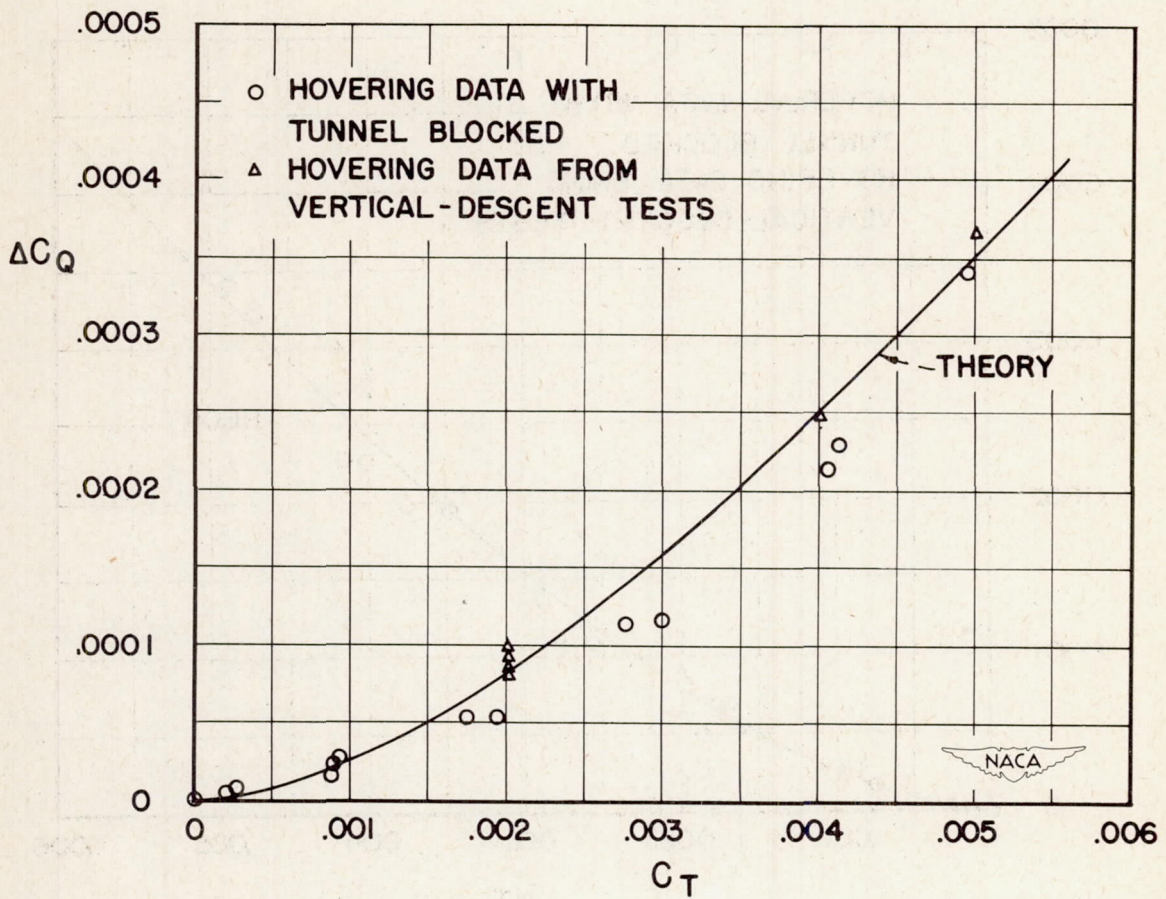
Figure 29.- Comparison of hovering data for 6-foot-diameter rotor with 3/1 tapered blades.

Figure 30.- Comparison of hovering data for 4-foot-diameter rotor with constant-chord, untwisted blades.

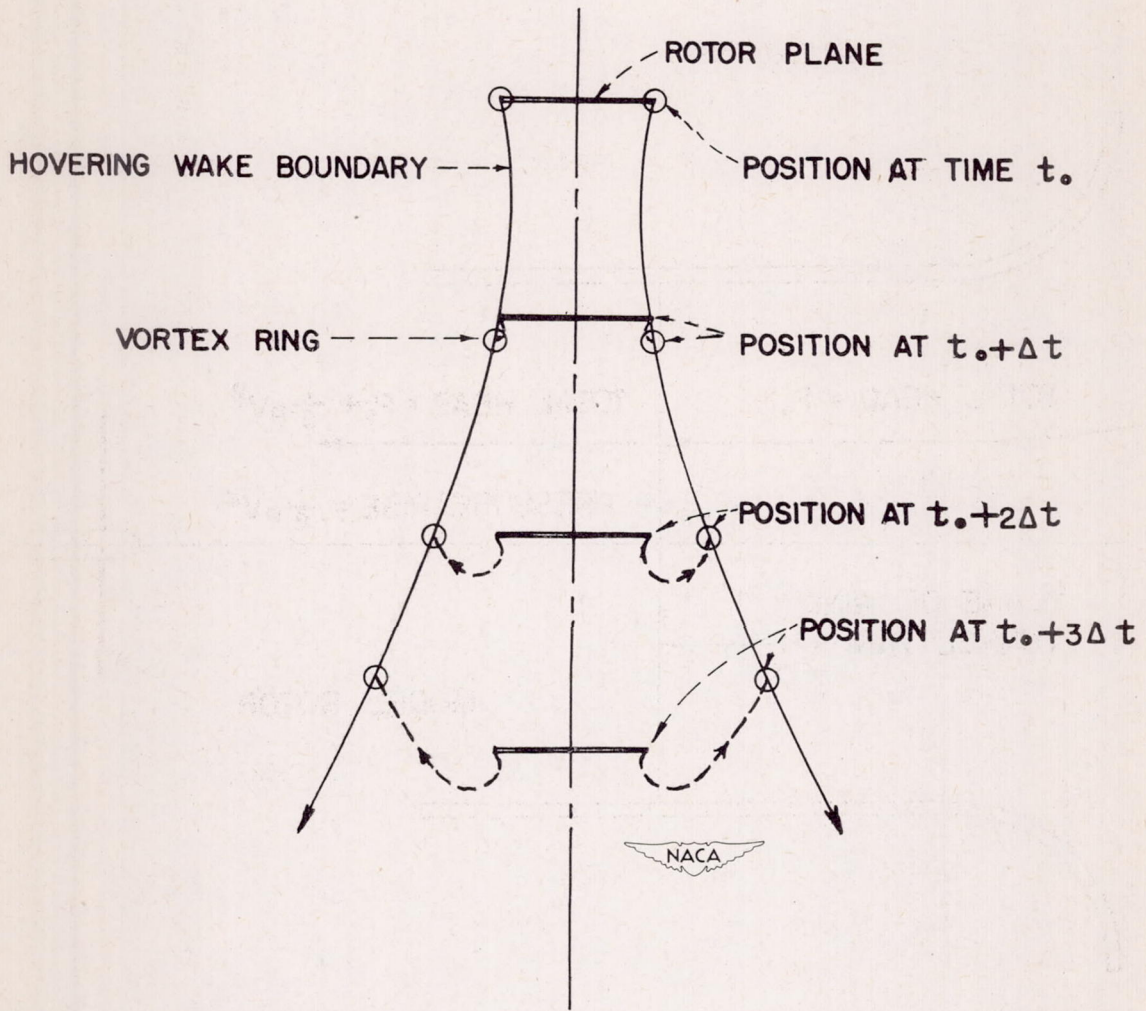Figure 31.- Schematic flow pattern for an actuator disk at small rate of descent in perfect fluid.

Figure 32.- Schematic sketch of transition from hovering to "vortex ring" type flow pattern. (Spread of wake is exaggerated.)
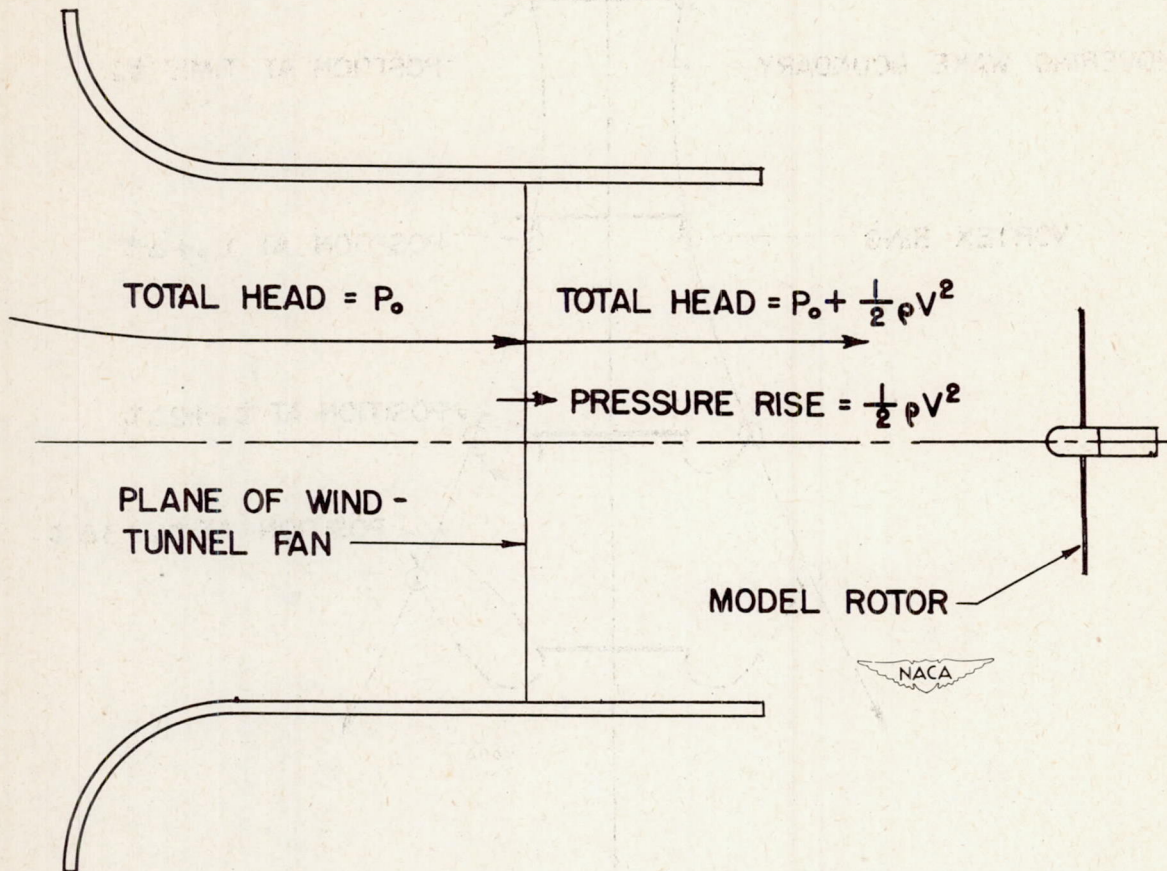
Figure 33.- Hypothetical frictionless, open-return wind tunnel.